The Pennsylvania State University

The Graduate School

Department of Electrical Engineering

VALIDATION OF LINEAR POLYFRACTAL ARRAYS AND THE OPTIMIZATION OF ANTENNA ELEMENTS IN AN INFINITE ARRAY ENVIRONMENT

A Thesis in

Electrical Engineering

by

Micah Dennis Gregory

Submitted in Partial Fulfillment
of the Requirements
for the Degree of

Master of Science

December 2009

The thesis of Micah Dennis Gregory was reviewed and approved* by the following:

Douglas H. Werner
Professor of Electrical Engineering
Thesis Advisor

Pingjuan L. Werner
Professor of Electrical Engineering

W. Kenneth Jenkins
Professor of Electrical Engineering
Head of the Department of Electrical Engineering

*Signatures are on file in the Graduate School

ABSTRACT

In recent years there has been much research into increasing the operating bandwidth of radio frequency systems. The need for wideband systems arise through demand for high data rate communications, multi-frequency radars, and other multipurpose communications devices. In addition to the circuitry of such systems, the antenna is an important component as well for energy to be effectively radiated over large operating bandwidths. Many designs and optimizations have focused on creating wideband antennas operating in isolation, but arrays are attractive because of the electronic beam steering capabilities and high gain properties that they exhibit.

This thesis covers two aspects of wideband antenna array design. The first topic is the arrangement of antenna elements in an array to maintain low relative sidelobe levels over a wide bandwidth. The most common configuration, the periodic array, generates grating lobes when the elements are electrically far apart. Grating lobes are portions of the array factor with power equal to the main beam; they cause energy transmission in undesired directions. Arranging the elements in an aperiodic fashion often has the benefit of reducing sidelobe levels over extended bandwidths if designed properly. The method used for aperiodically arranging elements is important to realize arrays with sufficient sidelobe suppression over a useful bandwidth. The recently introduced polyfractal array design approach is one successful method. Using the recursive nature of fractals and a powerful optimization technique, arrays exhibiting ultra-wideband performance with very low sidelobe levels have been created. The focus of the work presented here is to validate the effectiveness of polyfractal arrays consisting of real antenna elements. To this end, two small polyfractal arrays have been optimized, fabricated, and examined for wideband performance.

The second topic is the optimization of elements that are arranged in an infinite planar periodic structure. Arranging elements periodically allows easy of manufacturing and implementation. Although the upper frequency of operation is limited by the occurrence of grating lobes, large bandwidth percentages can be had if the antenna element is designed properly. Often, antenna arrays are created by designing a single element and placing it in an array configuration, though this comes with certain consequences. For instance, the antennas can shift their resonant frequencies and input return loss can become poor because of mutual coupling between elements. In addition, performance can become severely degraded when arrays are scanned, especially close to grazing angles. For these reasons, it becomes advantageous to design and optimize the antenna elements while they are in an array. In this manner, any effects due to nearby elements are automatically accounted for. Specialized simulation software along with a genetic algorithm is used for this purpose, creating effective wideband radiating elements to be used in planar microstrip phased arrays. The methods of antenna design and optimization are covered and two examples are presented and validated using a commercial electromagnetics simulation code.

TABLE OF CONTENTS

LIST OF FIGURES

LIST OF TABLES

ACKNOWLEDGEMENTS

The bases of this research and thesis were drawn from prior work by Dr. Joshua Petko, Robert Shaw, and Dr. Douglas Werner. The polyfractal array fabrication was inspired by research and results from the work of Dr. Petko. Through reviews of various publications on polyfractal array theory, it was clear there was an interest in how well the designs perform with real antennas. The work done here is mainly a response to that in addition to our own curiosity. Research on element optimization in an infinite array began with work by Mr. Shaw. Work was continued here at Penn State by the author after Mr. Shaw had graduated.

Chapter 1

Polyfractal Antenna Arrays: A Brief Overview

Linear polyfractal antennas arrays, a variation of fractal-random arrays, were first introduced by Petko and Werner in [1]. Since then, advanced methods of optimizing polyfractal arrays have arisen. In [2], the genetic algorithm was tailored to better suit polyfractal arrays by implementation of autopolyploidy. This yielded arrays with even better bandwidth performance. Most recently, multiobjective Pareto genetic algorithm (GA) optimization has been used to tailor performance for arrays where are there are multiple bandwidth goals [3]. Polyfractal arrays focus on the bandwidth issues associated with linear arrays of uniformly excited, isotropic radiators. There exists other array types where amplitude or phase adjustments are used to control the radiation pattern. However, amplitude and phase shading can significantly increase the complexity and cost of the antenna system.

1. 1. Shortcomings of Periodic Arrays

The most commonly used antenna array configuration is the periodic type. Here, a linear or planar arrangement of radiating elements are placed an equal distance apart from each other, the linear case shown in Figure 1-1. This simple arrangement has the advantage of being easily produced, but use is limited to narrow frequency bands, especially when beam steering is desired. This is due to the occurrence of usually undesirable multiple maxima in the array factor when element spacing is greater than one electrical wavelength [4]. This undesired radiation, called *grating lobes*, can cause significant problems in array systems . For instance, when the arrays are used in direction-critical applications such as radars, reflection readings from unintended angles can occur [5]. Figure 1-2 shows the array factor of a uniformly excited, 25 element, linear periodic array with element spacings of λ/2, 3λ/2, λ, and 2λ. If the array's minimum operating frequency was at λ/2 spacing (which is typical for mutual coupling reasons), this would correspond to operating frequencies of f_0, $1.5f_0$, $2f_0$, and $4f_0$. In the figure, the bottom axis represents the θ-axis in the plane of the array factor.

The equation for the array factor of an *N*-element, uniformly excited linear array is shown in (1-1), where β is the free-space wavenumber and d is the spacing between elements. To obtain the full radiation pattern for an array of a particular antenna, the pattern of a single element is multiplied by the array factor at each (φ, θ).

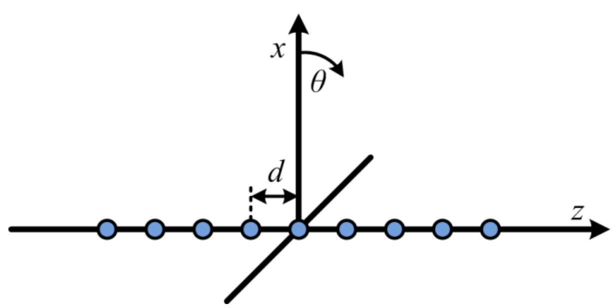

Figure 1-1: Linear periodic array configuration with uniform element spacing, *d*.

$$AF(\theta) = \sum_{n=1}^{N} e^{j\beta n d \sin\theta} \tag{1-1}$$

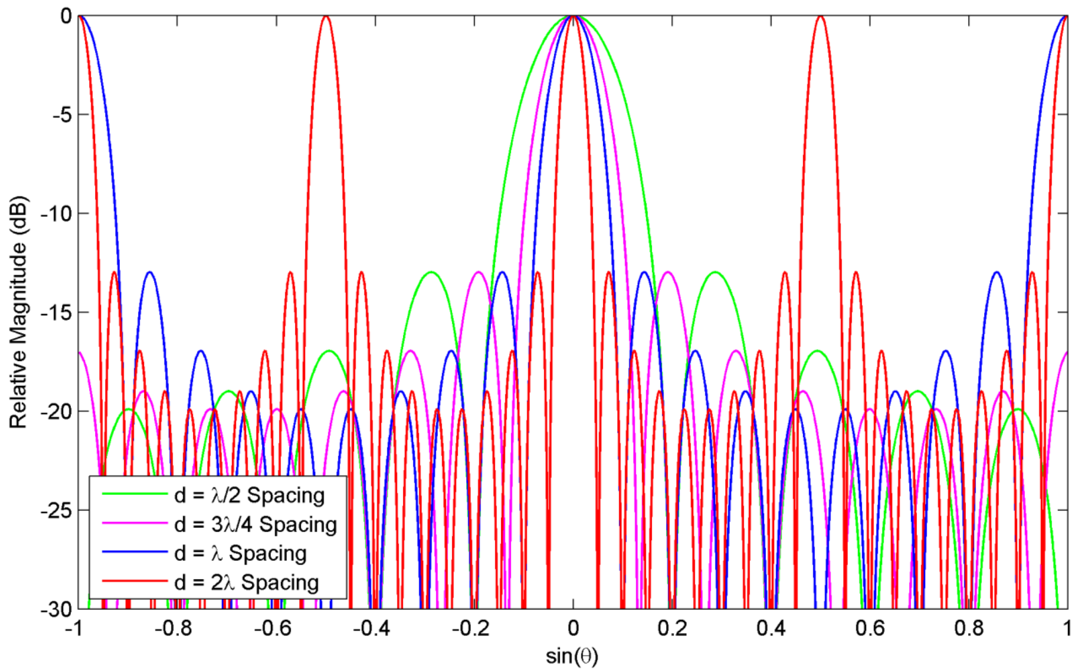

Figure 1-2: Array factors for a 25-element periodic array at various operating frequencies. Elements are uniformly excited and steered to broadside ($\sin\theta = 0$). Grating lobes appear at 1λ minimum spacing and larger.

From Figure 1-2 it shows that grating lobes first appear at $d = \lambda$ spacing when elements are steered to broadside, corresponding to $2f_0$ operating frequency. More grating lobes appear as the frequency is increased or if the array is scanned. Arrays with periodically spaced elements develop grating lobes when their element spacing exceeds $d = 1/(1+sin\theta)$ wavelengths, where θ is the beam scan angle from broadside [3], [6]. The array factor patterns in Figure 1-2 are essentially shifted left or right when the array is scanned; one can observe how a grating lobe that was previously in the invisible region of the array factor can be moved into the visible region when the main beam is steered. Grating lobes of periodic arrays are the main motivation for investigations into wideband arrays. These arrays attempt to suppress these lobes as much as possible for as wide an operating frequency as is desired or possible.

1. 2. Polyfractal Design Technique

The polyfractal array is a special subset of the fractal-random array [1], which first arose from Kim and Jaggard in [7]. Instead of fully determined fractal arrays, the fractal-random array uses more than one type of generator to form the structure. Depending on the number of generators and stages of the structure, the total number of possible outcomes of the final array can become quite staggering. The polyfractal array stands out from the fractal-random array in that the generator trees are not randomly connected together, but rather each generator tree specifies what tree is connected on the next stage by a set of connection factors. This implies that, with a specified set of generators (including connection factors) and number of stages, the array is fully determined. Changing the generator properties, often a relatively small set of parameters, changes the structure of the entire array [1]-[3]. Because of this, the genetic algorithm (GA) is well-suited to optimize these arrays [8]. It can effectively manipulate the generator properties until an array of suitable performance is obtained.

1. 2. 1. Polyfractal Array Method

The design of a polyfractal array begins with the definition of generators. Like a deterministic fractal and fractal-random array, the iterative application of these generators can lead to much larger structures [9]. Figure 1-3 gives an illustration of the how the arrays are built from a set of generators. Although the specification of connection factors reduces the available array configurations from the fractal-random superset, there is still significant variability in the polyfractal design such that a suitable wideband array can be found. Another advantage and differentiating characteristic of the connection factors is the ability to rapidly determine the array factor of the structure. Similar to a deterministic fractal array, there are great commonalities in the how the array is constructed that allow the array factor to be quickly calculated by finding the array factors of the generator structures as shown in Figure 1-4.

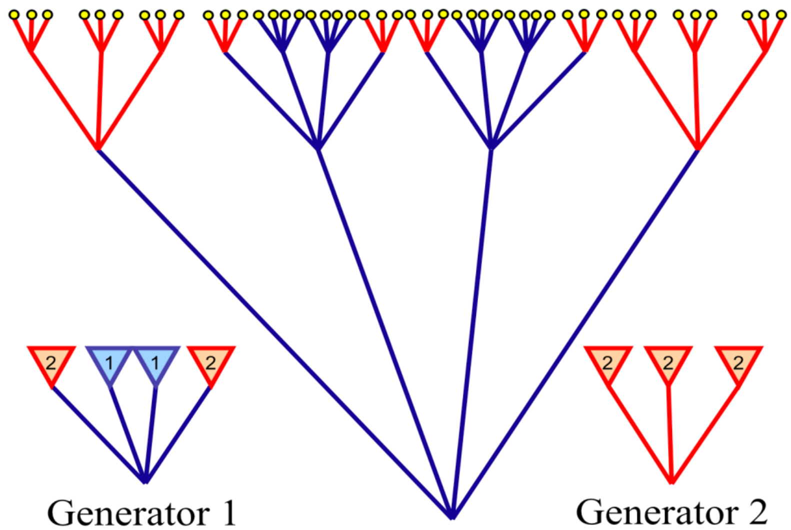

Figure 1-3: Example of a 46-element, 3-stage polyfractal array with the definition of two generators. The numbers on the ends of the generator represent the connection factors. For instant, the left branch on generator 1 will have a type 2 generator attached to it on the next stage [1].

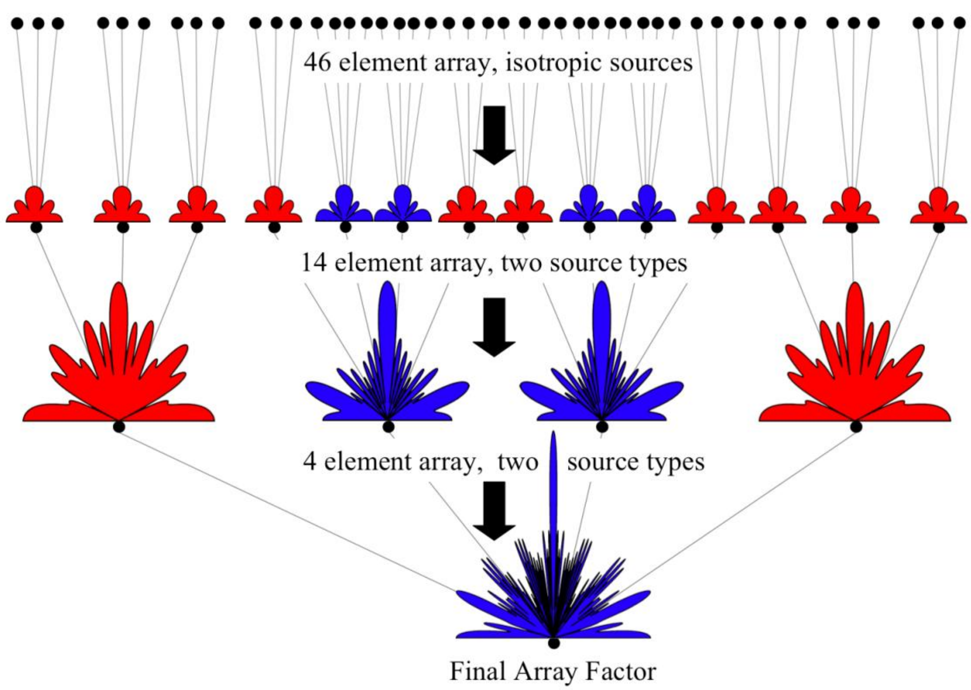

Figure 1-4: Recursive beam-forming of the array in Figure 1-3. The array factors of each generator needs to be calculated only once to determine the array factor of the entire array [1].

1. 2. 2. Special GA Operators and Multi-Objective Optimization

During ongoing research and experimentation with polyfractal arrays, special modifications were made to the genetic algorithm in order to obtain arrays with better performance. That is, arrays that exhibit lower sidelobe levels over extended bandwidths. A new GA operator was introduced in [2], termed *autopolyploidy* from the biological concept in which the amount of genetic material in an organism would increase while the organism remained essentially the same. Nearly the same occurs when applied to the genetic algorithm. For a population that is described by N generators (yielding N different arrays), a new population of 2N generators would form with N pairs of equivalent generators, all separately controllable via their new set of parameters. After this operation, the new chromosome (now double in length) will undergo mutation via a perturbation process to increase genetic diversity. Generator autopolyploidization is typically applied during the optimization after several generations that yield little increase in fitness. In this manner, the optimization can fruitfully continue where it may have previously converged.

In addition to autopolyploidy, multi-objective scenarios were implemented with a Pareto optimization technique, the strength Pareto evolutionary algorithm (SPEA) [3]. Instead of targeting a single bandwidth sidelobe level goal, the optimization targets two or more bandwidths. The solutions lay on *fronts* corresponding to their relative fitness values; the best performing members form the non-dominated set which belong to the *Pareto front*. A population member belongs to the Pareto front if no other population member has better fitness for all the design objectives. When using a multi-objective optimization tool, the user must decide at the conclusion of the process which population member of the Pareto front to select as the "winner". Because of the inherent trade-offs of the multi-objective scheme, this selection can change with different intended end-uses of the arrays.

1. 2. 3. Large Array Example

In the same manner that the small array in Figure 1-3 is constructed and evaluated, larger arrays can be created. In large arrays, the rapid beamforming in Figure 1-4 becomes very advantageous, offering computational times of a fraction of what would be required when finding each element's contribution to the final array factor [1]. In fact, arrays consisting of several thousand elements can be efficiently optimized with the recursive beamforming technique. The element locations of an optimized, 1924-element array is shown in Figure 1-5. The array bandwidth is shown in Figure 1-6 with an array factor at $f = 28f_0$ shown in Figure 1-7.

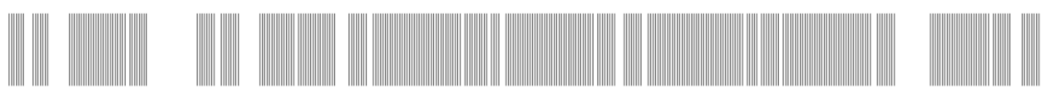

Figure 1-5: Array layout of a 1924 element optimized Polyfractal array.

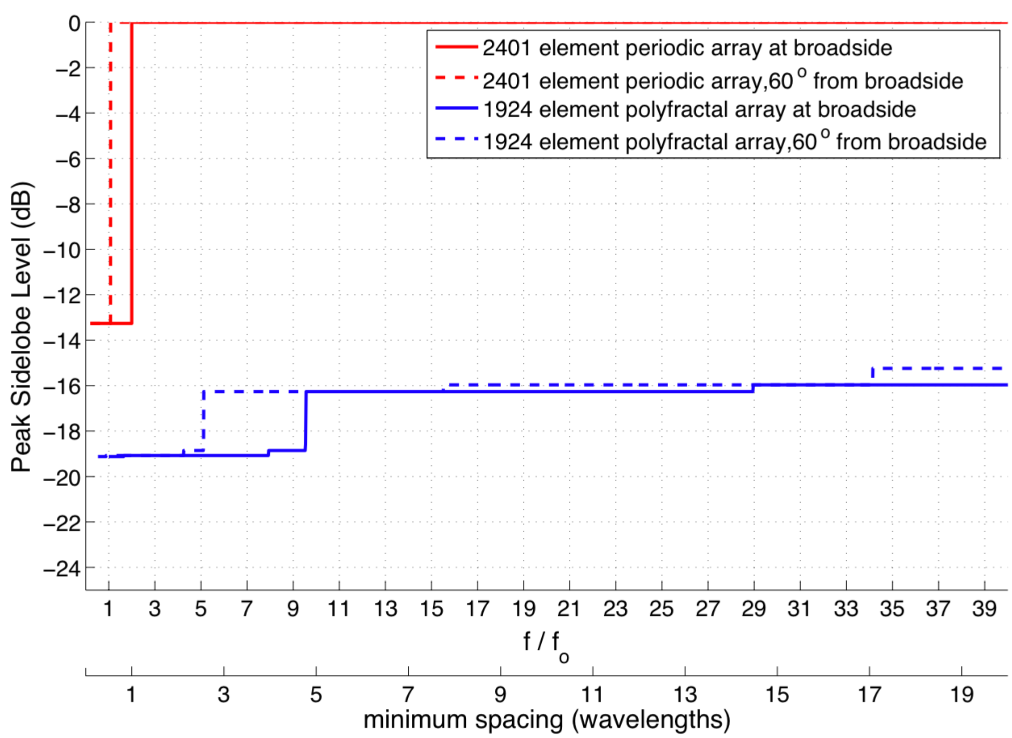

Figure 1-6: Sidelobe level of the example Polyfractal array and an equivalently sized periodic array. The Polyfractal array maintains very low sidelobe levels up to a 40:1 frequency bandwidth and beyond even when scanned. Conversely, the periodic array exhibits grating lobes at $f = 2f_0$ when steered to broadside and at an even lower frequency when scanned.

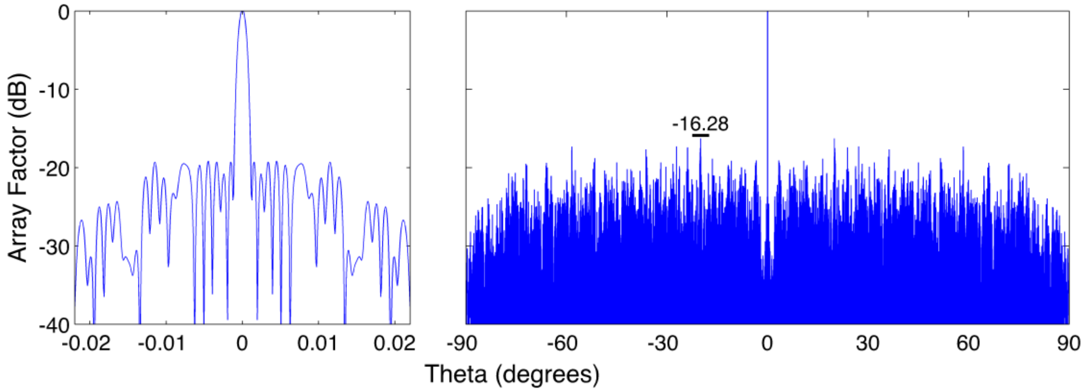

Figure 1-7: The array factor of the 1924 element Polyfractal array when operated with a minimum element spacing of 14 λ ($f = 28f_0$). The maximum sidelobe level at this frequency is -16.28 dB with respect to the main lobe.

Chapter 2

Fabricated Prototype Polyfractal Arrays

To prove the concept and performance of polyfractal arrays, two were constructed and tested. The two prototype arrays were of a small number of elements, only 32 each, to keep costs of production down. The arrays were optimized using a Pareto GA with autopolyploidy at minimum spacings of λ/2 and 2λ, corresponding to operating frequencies f_0 and $4f_0$, respectively. Figure 2-1 and Table 2-1 and show the final Pareto front of the optimization with the chosen members highlighted. One member was chosen for good performance at λ/2 and 2λ spacing (Array A) and another was chosen for best performance at 2λ (Array B). Figure 2-2 shows element locations of the two chosen members. The sidelobe level performance of the chosen members over an extended bandwidth is shown in Figure 2-3.

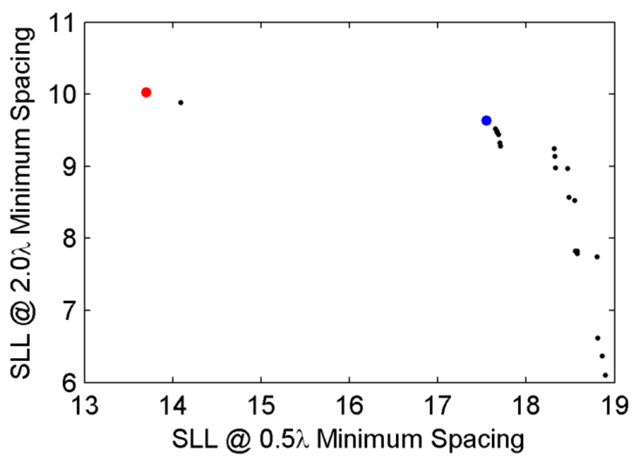

Figure 2-1: Final Pareto front of optimization with the two population members chosen for manufacturing highlighted in blue (A) and red (B).

#	λ/2 Spacing SLL (dB)	2λ Spacing SLL (dB)
1[B]	-13.7002	-10.0174
2	-14.0877	-9.8892
3	-17.5522	-9.6386
4[A]	-17.6473	-9.5208
5	-17.6676	-9.4929
6	-17.6716	-9.4658
7	-17.6842	-9.4371
8	-17.7016	-9.3298
9	-17.7058	-9.2722
10	-18.3146	-9.2499
11	-18.3222	-9.1415
12	-18.3317	-8.9816
13	-18.4789	-8.5724
14	-18.5459	-8.5301
15	-18.5537	-7.8278
16	-18.5546	-7.8278
17	-18.5749	-7.8253
18	-18.5779	-7.7857
19	-18.8021	-7.7444
20	-18.8051	-6.6179
21	-18.8584	-6.3654
22	-18.8917	-6.0997

Table 2-1: Final Pareto front population performance at optimization points. It can be seen that performance is often a tradeoff between the two goals. The selected prototypes are highlighted in blue and red for arrays A and B, respectively.

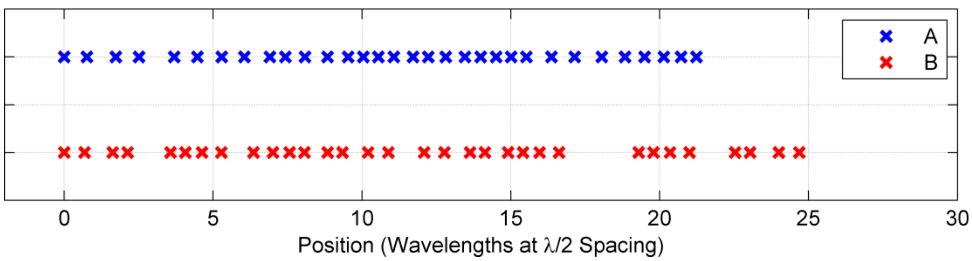

Figure 2-2: Normalized element locations for optimized example polyfractal arrays at the lowest operating frequency.

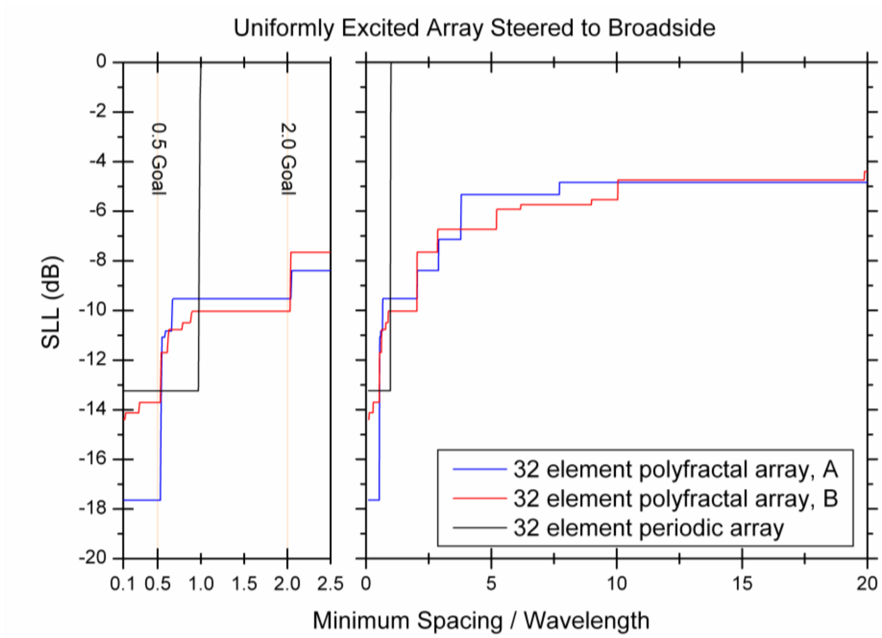

Figure 2-3: Sidelobe level versus minimum spacing for the two chosen members over an extended bandwidth.

2. 1. Array Factor Verifications

The most basic verification of the prototype arrays is performed by calculating the array factor in a mathematics suite. Here, MATLAB was used to compute array factors at different operating frequencies. Using the element locations created in the optimizations and a variation of array factor calculation in (1-1) [4], patterns for arrays A and B were generated and are shown in Figure 2-4 and Figure 2-5. The sidelobe levels for the two arrays are clearly much lower than the periodic arrays presented in Figure 1-2. The performance benefits of the polyfractal structure for even a small, 32 element array become obvious.

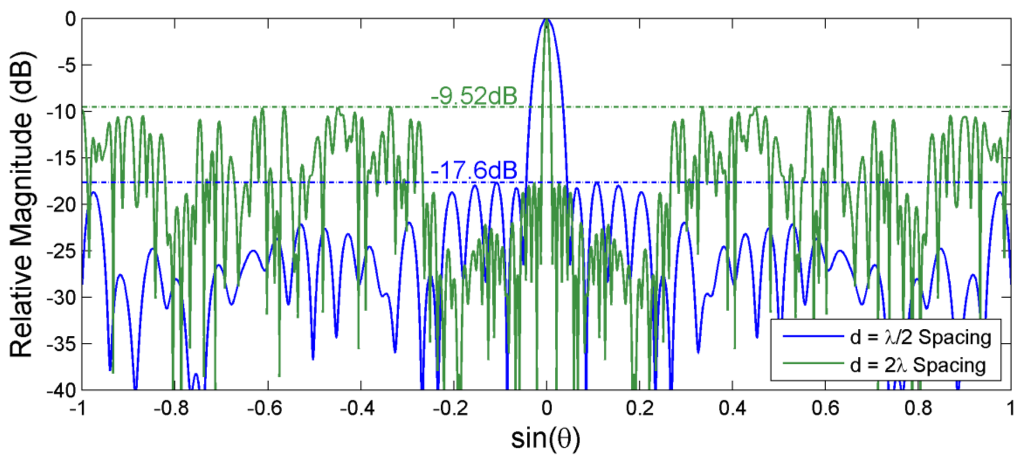

Figure 2-4: Array factor of example polyfractal array A at $\lambda/2$ and 2λ minimum spacing. Elements are isotropic, uniformly excited, and steered to broadside.

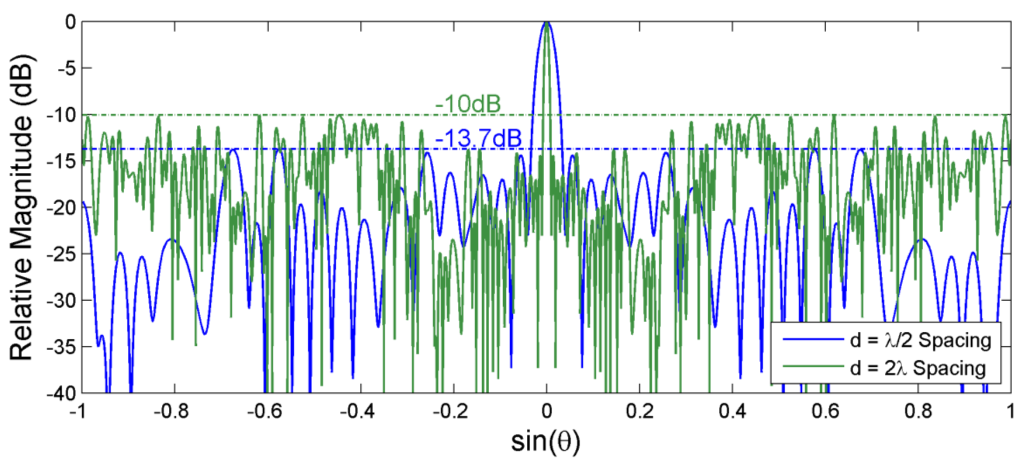

Figure 2-5: Array factor of example polyfractal array B at $\lambda/2$ and 2λ minimum spacing. Elements are isotropic, uniformly excited, and steered to broadside.

2. 2. Full Wave Simulations with Patch Elements and Feed Network

After computing and comparing array factors, the next step in verifying polyfractal performance is to merge the element locations from Figure 2-2 to actual radiating elements in a real array. Therefore, an antenna and array design topology must be selected to implement the design. The RF manufacturing technology of choice here is microstrip transmission line and patch antennas due to their low cost and ease of manufacturing [10]. Using printed circuit boards (PCBs) greatly simplifies testing and creates the best uniformity between antennas. PCBs also offer good tolerances so that patch elements are precisely where they need to be. The feed system for the array will be a standard corporate feed network. This allows a single generator to apply a uniform amplitude and phase signal to all the elements in the array. Ansoft Designer 2.2 [11] was used to analyze the entire antenna and feed network together. This method of moments simulation tool is designed for use with planar electromagnetic structures such as microwave PCB circuits and antennas; it is well suited to this design problem.

The fabrication facility was decided ahead of time to expedite manufacturing and testing. J. E. M. Manufacturing of Laurel, MD was chosen for their capability to build and test antennas in-house. One critical specification of the facility was a maximum PCB panel size of 17 inches on a side. With this knowledge, it is possible decide on the array's frequencies of operation. The element spacings at d_{min} = λ/2 (or f_0 operating frequency) determine the physical length of the array. In order to fit the largest polyfractal array (Array B) on a 17” panel, the minimum operating frequency would need to be at least 15.5 GHz. This would indicate a $4f_0$ operating frequency of 62 GHz. This upper frequency is a beyond the capability of today’s printed circuit substrates of reasonable cost. Significant losses and radiation from the corporate feed structure would make it very difficult to accurately measure the performance of only the antenna array. Therefore, it was decided to split each array into four sections, each section (or subarray) containing eight elements and their respective corporate feed network. At f_0 = 5 GHz, a 17 inch panel can comfortably fit even the largest subarray. Therefore, $4f_0$ is set to 20 GHz, still within the realm of microstrip antennas and feed networks. The element locations for the two arrays with the chosen operating frequencies are shown in Table 2-2.

Element #	Array A	Array B	Element #	Array A	Array B
1	0.0000	0.0000	17	0.7022	0.7247
2	0.0455	0.0408	18	0.7331	0.7655
3	0.1038	0.0975	19	0.7680	0.8170
4	0.1504	0.1275	20	0.8067	0.8470
5	0.2214	0.2139	21	0.8385	0.8938
6	0.2680	0.2439	22	0.8698	0.9238
7	0.3171	0.2772	23	0.8998	0.9572
8	0.3626	0.3164	24	0.9307	0.9963
9	0.4139	0.3811	25	0.9811	1.1566
10	0.4453	0.4202	26	1.0277	1.1866
11	0.4846	0.4536	27	1.0826	1.2200
12	0.5301	0.4836	28	1.1291	1.2591
13	0.5715	0.5304	29	1.1686	1.3511
14	0.6024	0.5604	30	1.2073	1.3810
15	0.6324	0.6119	31	1.2422	1.4392
16	0.6637	0.6527	32	1.2731	1.4800

Table 2-2: Physical element locations (in meters) for polyfractal array prototypes A and B when a minimum operating frequency of 5 GHz is chosen.

Since designing an antenna element and corporate feed matching network to work at both 5 GHz and 20 GHz is an additional significant design challenge in itself, instead two versions of each A and B polyfractal antennas were created, one to operate at each frequency. Simple square patch antennas with an impedance of 100 Ω were used; one patch for each operating frequency was parametrically optimized in Ansoft Designer. To keep the substrate electrically thin, 0.031 inch thick Rogers RT/Duroid 5880 was used. This material was used for its low loss properties and low dielectric constant of 2.2. The square patch element structures are shown in Figure 2-6 and Table 2-3. The bottom of the printed circuit substrate is a solid filled 1 ounce (0.0014 inch thick) copper ground plane. Simulated VSWR for the 5 GHz patch is 1.09:1 with a 100 Ω input port and gain is 6.87 dBi. The 20 GHz patch has a VSWR of 1.06:1 and a gain of 6.76 dBi.

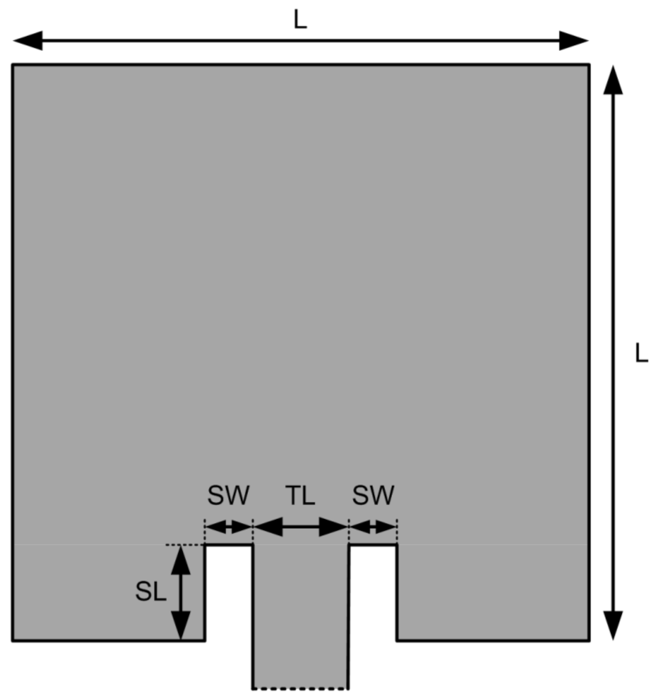

Figure 2-6: Dimensional references for the parametrically optimized square patch radiating element. The patches are designed for an input impedance of 100 Ω with a 0.031" thick substrate of Rogers RT/Duroid 5880 material with a solid copper ground backing.

Dimension	***f_o* (5 GHz)**	**4*f_o* (20 GHz)**
L	20.05 mm	4.77 mm
SW	1.85 mm	0.92 mm
SL	4.5 mm	1.145 mm
TL	0.62 mm	0.62 mm

Table 2-3: Optimized dimensions for the 5 GHz and 20 GHz square patches.

Quarter-wave transmission line matching sections are used in the corporate feed network to match the 50 Ω load where transmission lines join together back to 100 Ω. Only at the point of corporate feed input is there no matching section since a 50 Ω generator is specified. A silhouette of a corporate feed section at 5 GHz is shown in Figure 2-7. Corners of the feed network are chamfered to mitigate the effects of edges in the transmission line. The full array arrangements for prototypes A and B at 5 GHz and 20 GHz can be found in Appendix A.

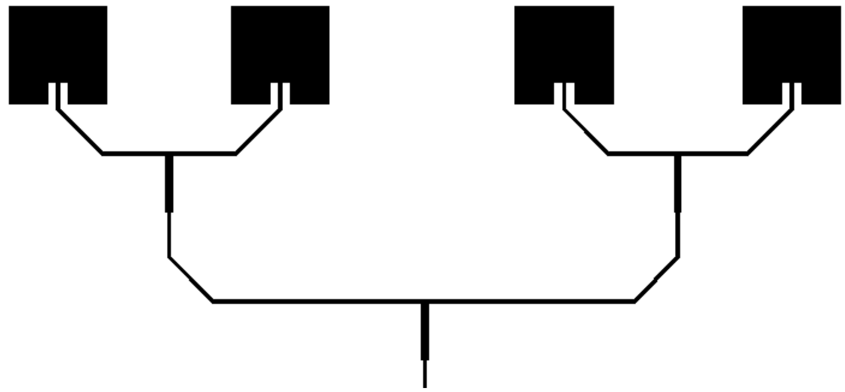

Figure 2-7: Partial section of corporate feed network and patch array for use at 5 GHz.

Since it was known prior to manufacturing that the arrays would be split into groups of subarrays, the prototypes were simulated in two fashions. One set of simulations was done with the entire 32 element arrays and the full corporate feed, and another with subarrays and partial corporate feed sections. The electric field of the radiation patterns from the subarray method are combined with Equation 2-1, where *n* is the subarray number, *k* is the free space wavenumber, and d_n is the position of subarray *n*.

$$E_{\varphi,total}\,(\theta) = \sum_{n=1}^{4} \left|E_{\varphi,n}\,(\theta)\right| e^{j\left[angle\,\left(E_{\varphi,n}\,(\theta)\right) + kd_n\,\sin\,\theta\right]} \quad (2\text{-}1)$$

One immediate advantage to the subarray fabrication and measurement as opposed to the full array method is that the radiation pattern data can be more accurately gathered. With fewer elements in the arrays, the radiation pattern has lower $|\delta E_{\varphi}/\delta\theta|$, which signifies that sidelobes are easier to pick out and accurately measure with a limited $\Delta\theta$ of the antenna rotation mechanism. In addition, a large section of the corporate feed network is removed that would have originally fed the 8-element groups. Loosing these large lengths of microstrip transmission line reduces feed line radiation and losses, leading to a more accurate measurement of the radiation pattern due solely to the patch antennas. The radiation pattern differences between pattern combination of subarrays and simulating the entire arrays is shown in Figures 2-8 and 2-9. It can be seen that the radiation of the large section of transmission line feeding the subarrays can have a beneficial or detrimental effect on pattern sidelobe level. Even with the additional radiation of the corporate feed, the arrays maintain low sidelobe levels, especially at 20 GHz where a periodic array would develop several grating lobes across the pattern.

(a)

(b)

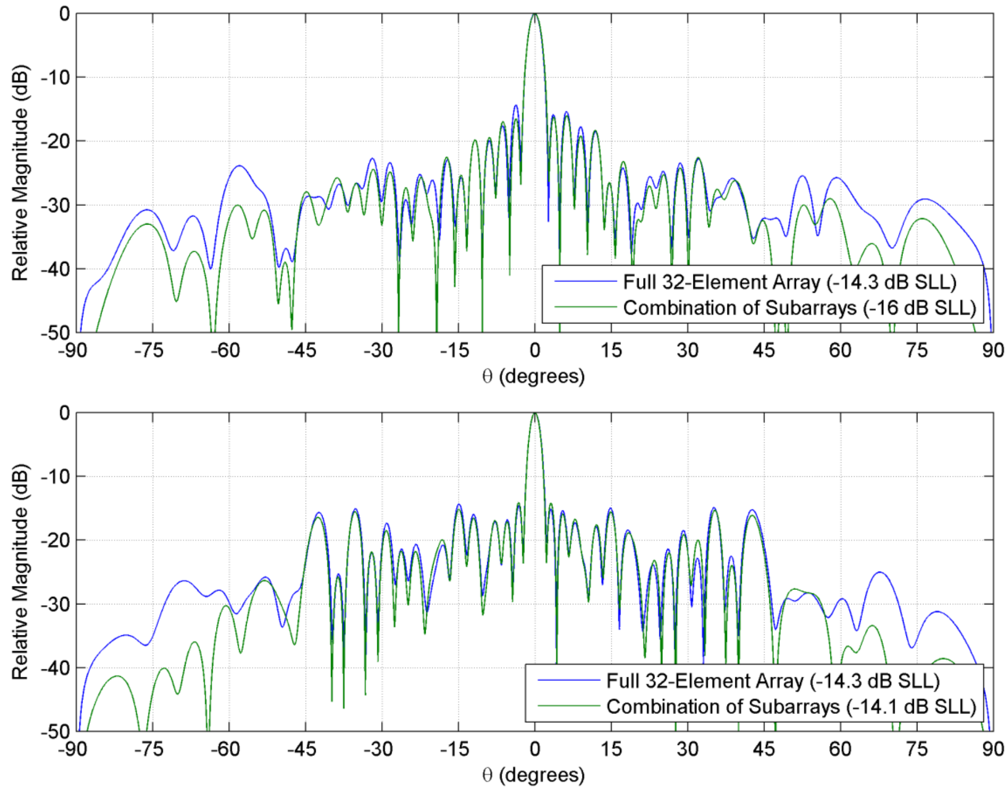

Figure 2-8: Simulated radiation patterns at 5 GHz of the full 32-element array A (a) and array B (b) with full corporate feed network (blue) and of the combined patterns of subarrays (green). The difference in the two radiation patterns is due solely to the length of transmission line that feeds the subarrays.

(a)

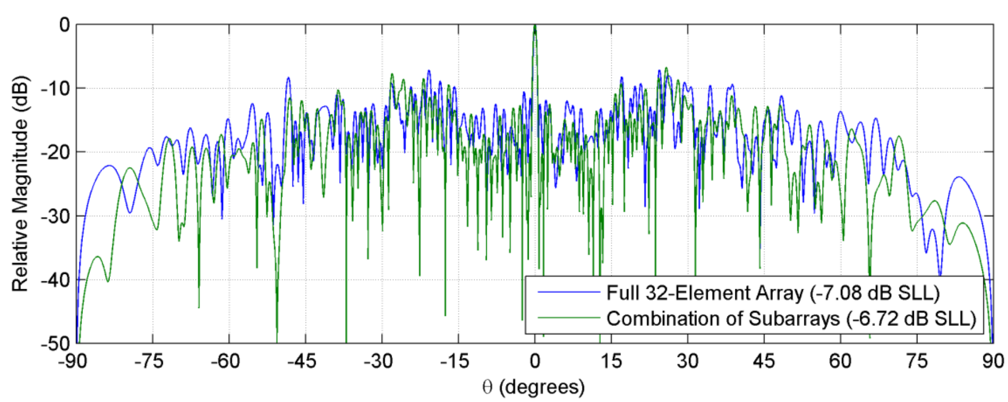

(b)

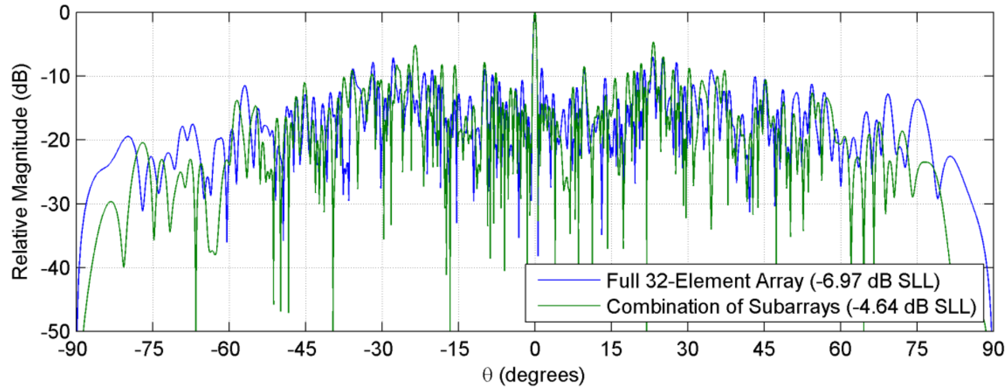

Figure 2-9: Simulated radiation patterns at 20 GHz of the full 32-element array A (a) and array B (b) with full corporate feed network (blue) and of the combined patterns of subarrays (green). The difference in the two radiation patterns is due solely to the length of transmission line that feeds the subarrays.

2. 3. Fabricated Arrays and Measurements

After the arrays were verified with Ansoft Designer, the designs were exported for manufacturing at J.E.M. Engineering of Laurel, MD where they would be measured as well. Electric field magnitude and phase information in the plane of the array factor was gathered for each subarray at their intended operating frequencies. The measured and simulated magnitude information for the subarrays of prototype A is shown in Figure 2-10 and Figure 2-11. The phase information of the electric field is not plotted since by itself it is not meaningful, but it is important in order to combine the subarray patterns together to create the full radiation patterns. One easily noticeable difference between the measured and simulated patterns is the magnitudes near the zenith ($\theta = \pm 90°$). This occurs because the simulated radiation patterns assume an infinite ground plane, whereas the fabricated subarrays have a truncated ground. Photographs of the tops of the fabricated subarrays are shown in Appendices B and C. Not shown is the panel bottoms, which have solid copper plating and are electrically connected to ground at each panel's SMA connector input port.

The experimentally gathered magnitude and phase information from each group of subarrays is then combined using (2-1) in the same manner as that of the simulated subarrays. The compiled radiation patterns are shown in Figure 2-12 and Figure 2-13 and are compared with that of the combined-subarray simulated patterns in Figure 2-8 and Figure 2-9 since they most accurately reflect the experimental measurement circumstances.

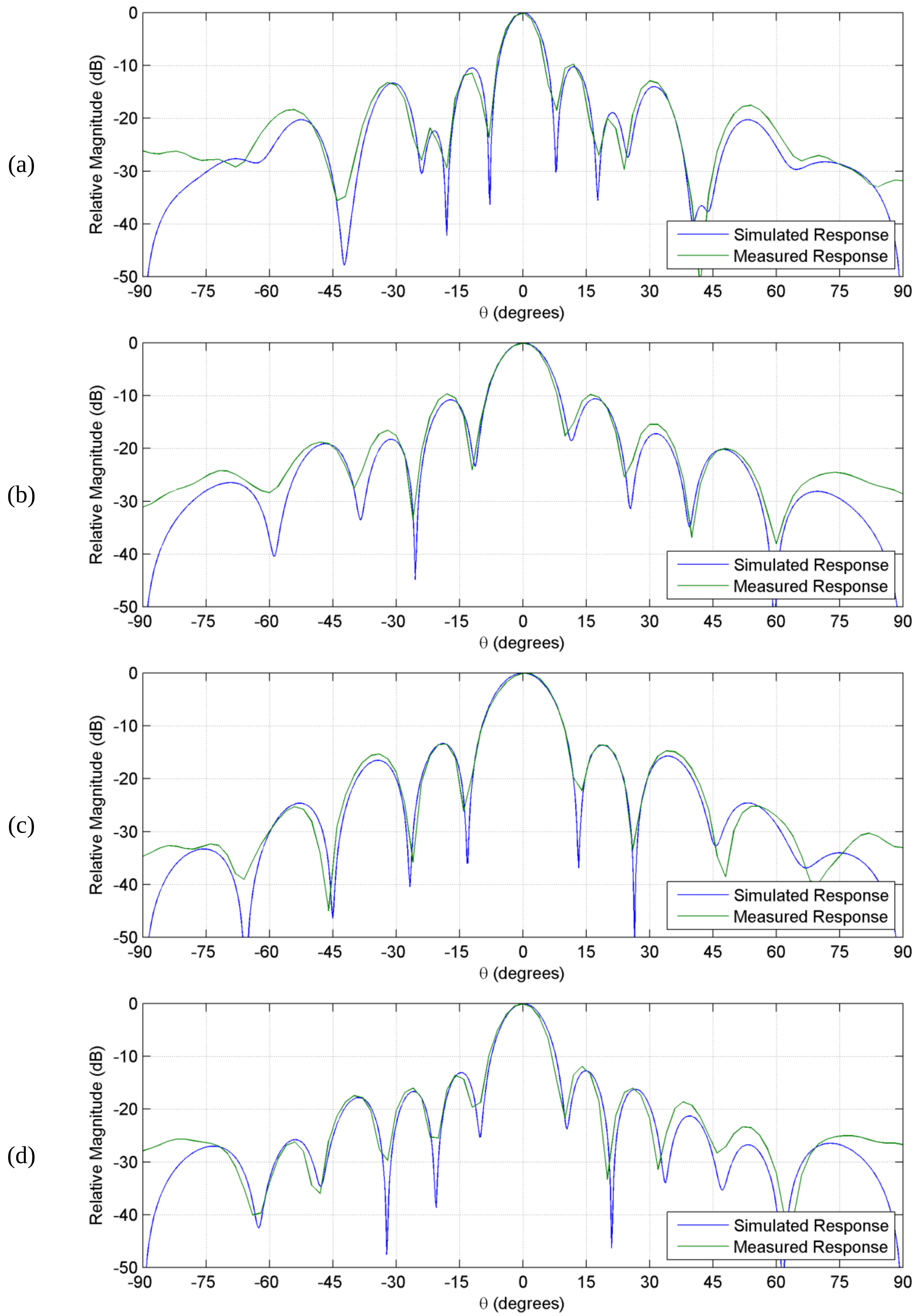

Figure 2-10: Radiation patterns at 5 GHz for subarrays one though four (a through d, respectively) of prototype A. Good agreement between simulations and measurements is obtained for prototype B at 5 GHz as well.

(a)

(b)

(c)

(d)

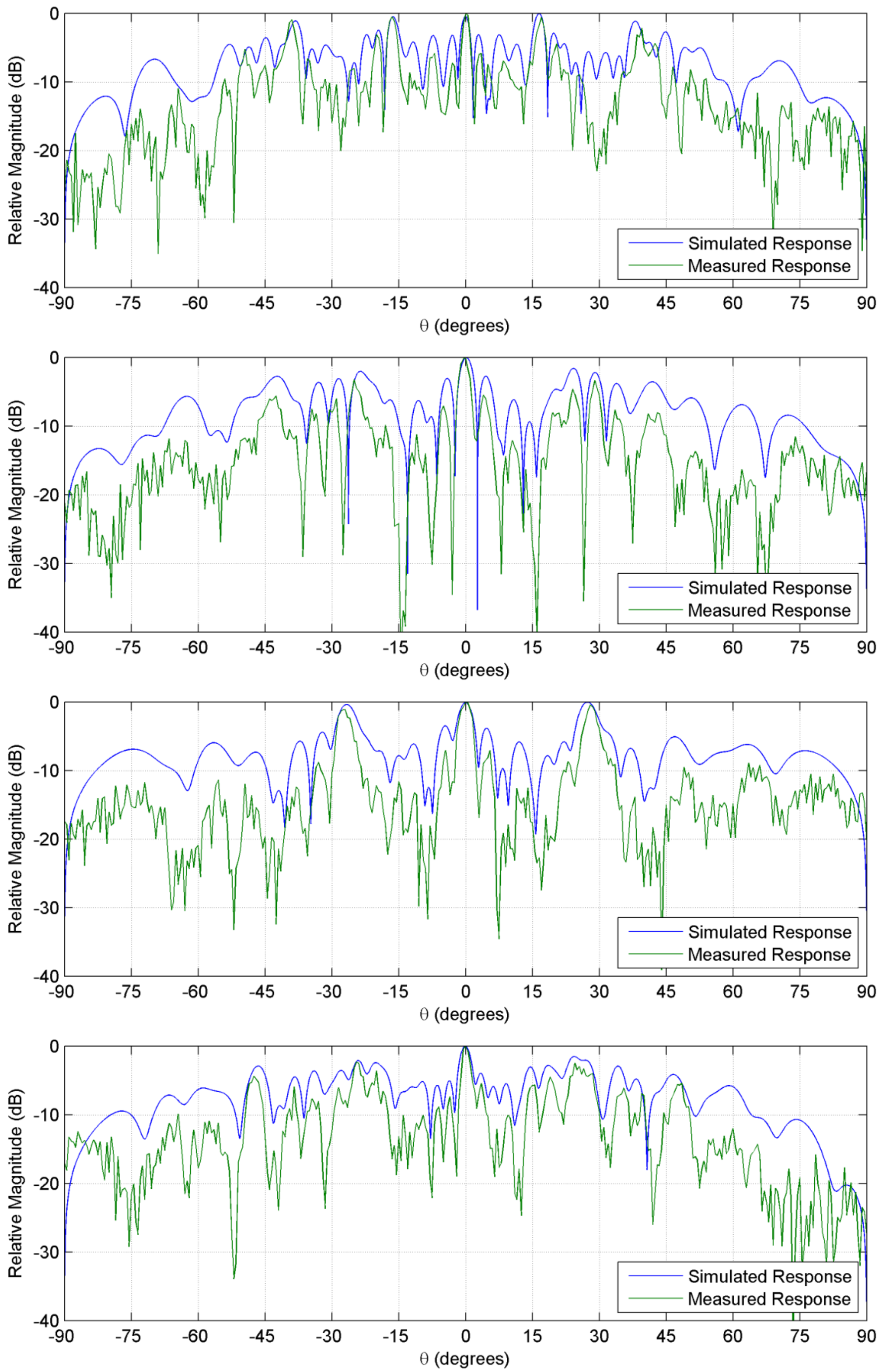

Figure 2-11: Radiation patterns at 20 GHz for subarrays one though four (a through d, respectively) of prototype A. The agreement between measurement and simulation at 20 GHz is not as good as that at 5 GHz, which can be expected due to increasing parasitic and non-ideal effects with increasing frequency. Prototype B shows similar patterns.

(a)

(b)

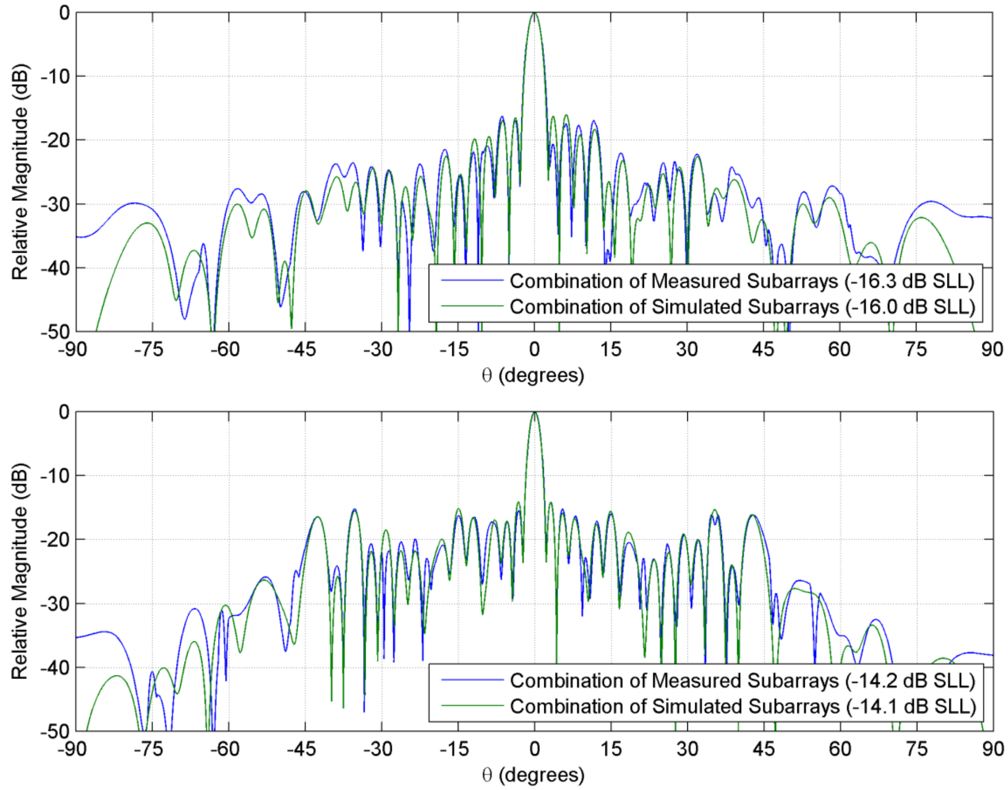

Figure 2-12: Full array radiation patterns for experimental prototypes (blue) and simulated arrays (green) for prototypes A (a) and B (b) at 5 GHz.

(a)

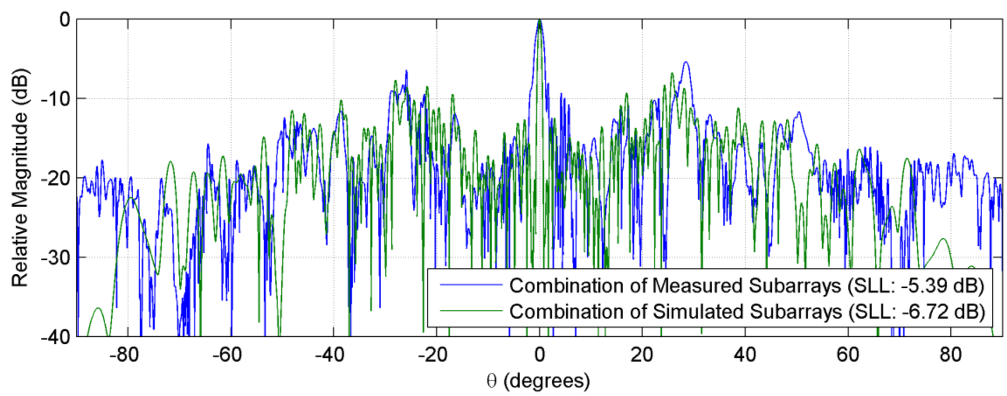

(b)

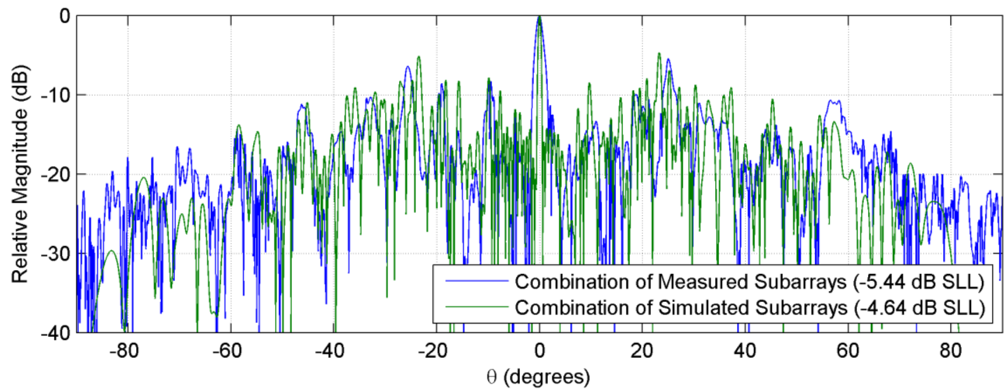

Figure 2-13: Full array radiation patterns for experimental prototypes (blue) and simulated arrays (green) for prototypes A (a) and B (b) at 20 GHz.

Both prototypes exhibit good sidelobe suppression at their intended frequency of operation. At f_0 (5 GHz, Figure 2-12), the polyfractal arrays have sidelobe levels lower than that of periodic arrays, even where periodic arrays excel (when $d_{min} = \lambda/2$). At frequencies where element spacing is larger than λ (where wideband arrays become useful), the polyfractal prototypes still give good sidelobe suppression and exhibit no grating lobes. At the upper operating frequency ($4f_0$), a periodic array would have grating lobes at $sin\theta = \pm 0.5$ ($\theta = \pm 30°$) and $sin\theta = \pm 1.0$ ($\theta = \pm 90°$) as shown in Figure 1-1. Although the nulls of the radiation pattern of the patch element would significantly attenuate the lobes at ± 90°, the lobes at ± 30° would still pose a significant problem. Here, the fabricated polyfractal prototypes yield sidelobes approximately 5.5 dB lower than the main beam and any grating lobes that a periodic array would exhibit.

The experimental and simulated radiation patterns for 5 GHz in Figure 2-12 show very good agreement and have excellent input impedances as evidenced by their measured VSWR shown in Table 2-4. The simulations and measurements do not agree as well with the 20 GHz prototype arrays, which can be attributed to several factors. The width of the main beam for the fabricated arrays is larger than that of the measured arrays. It is observed that the arrays, due to their diminutive thickness, can easily bow which can cause expansion or compression of the main beam. This issue becomes more prominent at higher frequencies, where geometrical anomalies of the fabricated arrays are of the same order as an electrical wavelength. Beam expansion can also occur because of the truncated ground plane, as mentioned before. Other differences in the radiation patterns can be attributed to a finite sized computational mesh used with Ansoft Designer's method-of-moments simulation code, measurement amplitude and phase error, and measurement observational angle error. In spite of these issues, the arrays still function as intended, yielding low sidelobe levels over a 4:1 bandwidth.

Array	Frequency	Subarray 1	Subarray 2	Subarray 3	Subarray 4
A	5 GHz	1.34	1.22	1.14	1.09
B	5 GHz	1.27	1.26	1.26	1.13
A	20 GHz	1.42	1.68	1.72	1.79
B	20 GHz	2.03	1.74	1.97	1.63

Table 2-4: Measured VSWR for the 16 separate subarrays.

Chapter 3

Antenna Element Optimization in an Infinite Array Environment

Another challenging aspect of wideband array design is the antenna elements themselves. There are always new types of wideband antennas being designed as the applications for them become more demanding and unique, so often such that no single antenna can fulfill all the necessary bandwidth, size, gain, or polarization requirements. For this reason, it is advantageous to have a design method where antenna requirements are included in an optimization procedure. Therefore, an antenna can be easily created for each application. This process will be applied here where antennas are placed in a periodic phased array. In addition to basic antenna design concerns, when antennas are in close proximity to each other (as in arrays), parameters such as gain and input impedances can be significantly different from those of the same antenna in isolation [4]. Therefore, it is unlikely to be able design an antenna that performs well in isolation, place that antenna in an array and expect it to perform similarly.

The amount of performance impact is related to the steering angle of the phased array and the distance between the antennas. It would stand to reason that antennas could be simply placed far apart to avoid this issue, but in the case of periodic arrays, the elements need to be placed closely together to prevent grating lobes from occurring as demonstrated in the Chapter 1. They must be spaced at a maximum of 1 λ apart to avoid grating lobes when steered to broadside and closer still for scanning [3]-[5]. Typically, elements are spaced $\lambda/2$ apart so they can be scanned all the way to end-fire without grating lobes. Placing them closer than $\lambda/2$ is not generally done because it offers no additional scanning range, mutual coupling effects become stronger [4], and radiating elements often occupy or are bounded by spherical areas with diameter on the order of

$\lambda_0/2$ for best efficiency, bandwidth, and gain [12], [13]. A simplified element spacing tradeoff curve is shown in Figure 3-1.

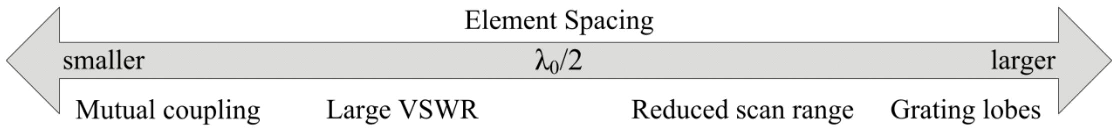

Figure 3-1: Performance consequences of element spacing in a periodic array.

Closely spaced antennas bring about the common design issue of mutual coupling. Much research has been invested in observing the effects of mutual coupling [14], [15], predicting, analyzing, and modeling those effects [15]-[19], and eventually attempting to compensate for or mitigate them [20]-[22]. It can be concluded from the amount of effort applied to tackling this effect that it is a significant problem with great theoretical and practical concern.

Most investigations into mutual coupling that attempt to quantify or explain the effects utilize simple microstrip antennas; these contain fairly straightforward field distributions which allow for the simplifications shown in [16]-[18]. Unfortunately, most wideband microstrip designs are comprised of complex geometries [23]-[28], making modeling and estimation of mutual coupling difficult. These antennas typically require a numerical simulation tool or experiments to determine coupling factors.

An excellent way to account for these factors is to simulate the antenna element as if it were in an array. A periodic finite-element boundary integral (PFEBI) program has been developed at the Penn State Computational Electromagnetics and Antennas Research Laboratory (CEARL) by Ling Li and Xiande Wang that is specifically designed to simulate structures in an infinite array environment [29]. It is commonly used to analyze frequency selective surfaces, and can be used to analyze antennas if a source is placed inside the structure instead of propagating a plane wave towards the surface. While an antenna is simulated in the array, all mutual coupling and other factors created by close-proximity neighboring antennas are accounted for via the periodic boundary conditions. Array scanning is accomplished by applying a phase shift between the parallel boundaries.

Additionally, the PFEBI is a computationally efficient code which can be easily bundled with an optimization technique. In this manner, an antenna with in situ antenna gain and input parameters can be optimized for use in an array with wide bandwidths, large scan angles, or other characteristics. A similar method is used with an alternative computational technique in [30], however certain design liberties are granted that typically do not allow cost effective construction. One is a very thick substrate material, which can make arrays very expensive and heavy. Another is that the optimizing algorithm is allowed to choose the system impedance that allows greatest bandwidth. This would require a matching transformer for the typical system impedances of 50 Ω or 75 Ω that operate over the necessary bandwidth. Additionally, the antennas require a balanced input for the self-similar metallic designs, however, the balun function could be integrated into the matching transformer.

In the following chapters, antenna elements are optimized with a genetic algorithm where they are effectively in an infinite array of identical elements. They are designed to allow beam scanning while retaining a large impedance bandwidths and high gain. Additionally, restrictions are placed on cross-polarized gain to ensure linear polarization. The intended end-use of the optimized elements would be wideband, easily manufactured phased array antenna systems with conical beam steering capabilities dictated by the goals of the design.

3. 1. Antenna Implementation in PFEBI

When creating an antenna in PFEBI, one essentially defines the finite element mesh through a set of input files. Unlike a commercial software program where the user specifies shapes and the software automatically meshes it, every finite element must be specified manually.

Although this can initially be challenging, once a coding scheme is implemented it allows for easy construction of complex structures through *pixelization*, where binary representations are mapped to create physical objects consisting of dielectrics, metal, or other complex impedance surfaces.

Antennas are constructed in PFEBI as shown in Figure 3-2. The program loads a series of ASCII text files that specify the metal and material structure, as well as dimensions, material properties, and simulation specifications. Each antenna element consists of a stack of cuboid material pixels N_X by N_Y wide and N_Z deep. Each of these material pixels can have different isotropic or anisotropic electric and magnetic properties, and lossy or perfectly conducting metal can specified on one or more of the six sides of each pixel.

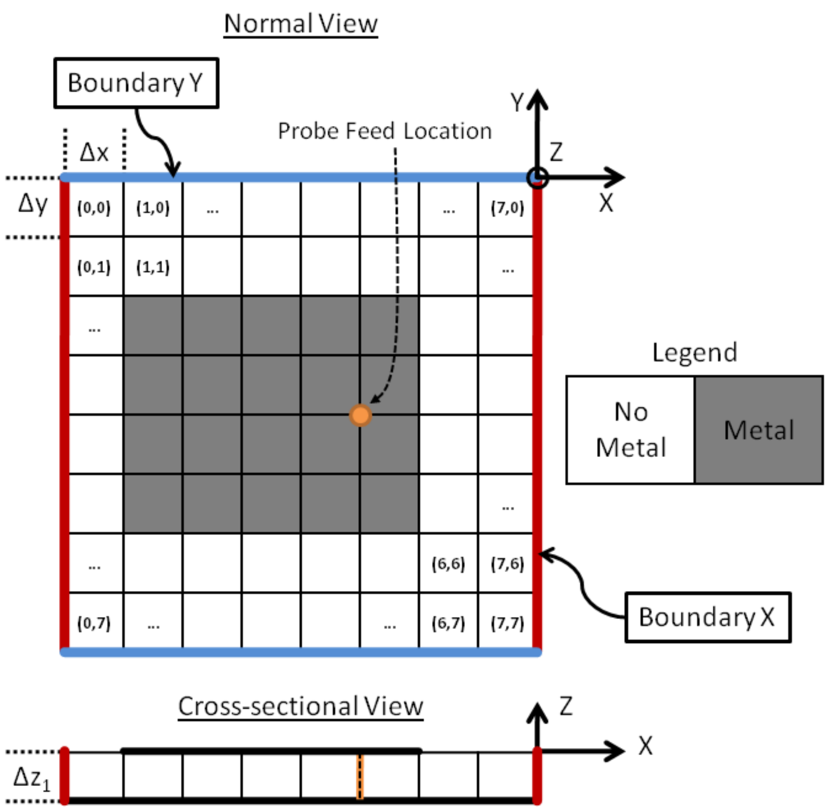

Figure 3-2: Basic antenna construction in PFEBI. In this example, $N_X = 8$, $N_Y = 8$, and $N_Z = 1$. Since the design has periodic boundary conditions, the red (X) borders are electromagnetically equal, as are the blue (Y) borders. Shaded pixels are metal, this design having a 5 by 4 pixel rectangular metal patch antenna in the X and Y dimensions, respectively. It is fed by a current source at the bottom right edge of pixel (4,3) in the z-direction spanning the single Z layer, Δz_1 thick. All pixels (0,0) to (7,7) in the Z_1 layer can have varying electric and magnetic properties, specified by $\varepsilon_{(x,y)}$ and $\mu_{(x,y)}$, where each can be complex, signifying loss.

Since the element spacing is typically $\lambda/2$ because of the restrictions illustrated in Figure 3-1, careful consideration of the unit cell size, which inherently determines spacing, must be taken. The X and Y dimensions of the unit cell are $N_X \cdot \Delta x$ and $N_Y \cdot \Delta y$, respectively; Δx and Δy must be equal for all X and Y pixels in their respective axis, however Δx and Δy along with N_X and N_Y can be different to form rectangular unit cells. Typically, $N_X = N_Y$ and $\Delta x = \Delta y$ to form a square lattice periodic grid and square antenna areas. Antenna bandwidth must be formed below the frequency and scan angle where grating lobes occur, therefore most optimized antennas will occupy a large area of the unit cell to operate effectively at these lower frequencies.

3. 2. Design Considerations

As with many commercial numerical electromagnetics solvers, there are import things to consider before simulation in order to get the proper and correct results. Mesh size, source excitation type, and verification are very important, to name a few. Each will be discussed in detail here as it applies to the appropriate simulation tool. Most design specifications and software considerations are compromises, often between code capability, speed, and user-friendliness.

3. 2. 1. Finite Element Mesh Size

The illustration in Figure 3-2 is a simplification of most design requirements. Since unit cells are typically $\lambda_0/2$ on a side, this would imply a $\lambda_0/16$ X-Y mesh size, which would be even more coarse in a dielectric material. Accuracy and S-parameter convergence studies with PFEBI have shown that a 60 by 60 X-Y mesh is an acceptable compromise between broadside and scanned accuracy and computational time. For these studies, typical dielectrics ranged from ε_r =

1.8 to 3.5 with no loss included. This dielectric range is also what is commonly used in the optimized antennas designed with the software.

Although using a small mesh size has increased computational time penalties, there is a silver lining. Much more complex metallic geometries can be created and it also allows for greater precision for critical objects such as microstrip lines and apertures. This enables the optimizing algorithm to create an antenna with better characteristics.

3. 2. 2. Source Excitation

When comparing the many different commercial electromagnetics software packages available, it is clear that there are many different ways of exciting a structure. For instance, HFSS™ allows voltage sources, current sources, lumped ports, wave ports, and so on. Careful choice of excitation must be exercised in order to get the proper results, and it is not always clear what excitation should be used in a certain situation. PFEBI uses a fixed current source embedded in the structure to excite the antenna. In order to determine the input impedance at that point, the voltage across the current source must be extracted. Although HFSS™ offers the same type of feed, the use of a lumped port in HFSS has shown excellent agreement with PFEBI and the software will automatically calculate impedance and S-parameters when using this, where with the current source, one would have to manually extract fields to find impedance.

The current source excitation of PFEBI is limited in that it can only span a single FE unit or pixel. In order to have a source that can span more than one material pixel, the current sources must be stacked, and the impedance calculated by the sum of the voltages across the sources. In this situation, all of the stacked current sources must have equal magnitude and phase excitation.

3. 2. 3. Validation of PFEBI Results

In order to confirm that the impedances and gains determined by PFEBI are in fact what a real antenna in the array would exhibit, Ansoft HFSS™ is used to verify each optimized antenna [31]. This commercial simulation code allows the same periodic boundary conditions that PFEBI uses, so comparison is fairly straightforward. Above and below the unit cell are boundary conditions dependent on the design. For antennas with a solid metal back plane (which is typically the case), the bottom boundary condition is a perfect electric conducting surface. Otherwise, both the top and bottom boundaries, which are located approximately a half-wavelength away from the surfaces, are perfectly matched layers. This is used instead of a normal radiation boundary, which causes reflections when the antenna is scanned far from broadside. An example of the simulation space and boundaries is shown in Figure 3-3. This type of antenna configuration is used for the verification of all of the antennas presented in chapter 4. HFSS™ is not generally used for optimizations due to the heavy computational requirements of the code. In this respect, PFEBI is much more efficient, although lacking many of the tools and features of HFSS™. It can be said that PFEBI is a tool designed for only a few specific purposes, but it performs them very efficiently and effectively.

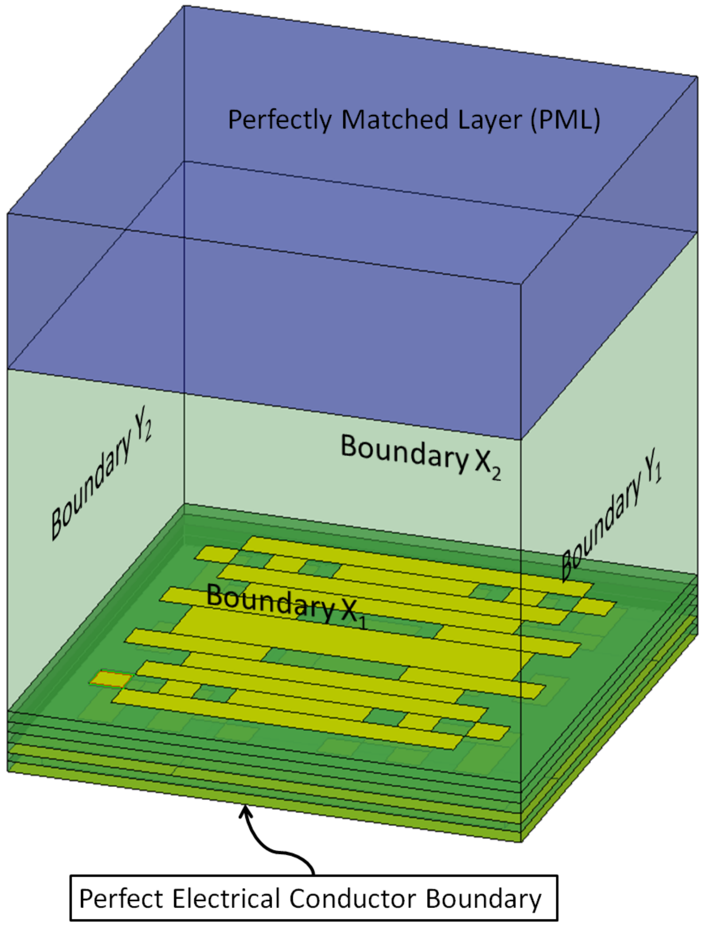

Figure 3-3: Antenna and boundary visualization in Ansoft HFSS™. Green represents substrate material and gold represents metal which is usually copper. For the periodic boundary conditions, boundary X_1 = boundary X_2 and boundary Y_1 = boundary Y_2. The bottom boundary is the antenna's ground plane, which is interpreted to be a perfect electrical conductor.

3. 2. 4. The Genetic Algorithm

The computational tool used to optimize the antennas is a binary genetic algorithm created by D. L. Carroll (version 1.7a). This genetic algorithm is designed to evaluate functions in parallel. That is, when used in a multithreaded environment such as a computer cluster, simultaneous evaluations of the population members are performed to reduce total optimization time. The simplified GA optimization process is shown in Figure 3-4 [8].

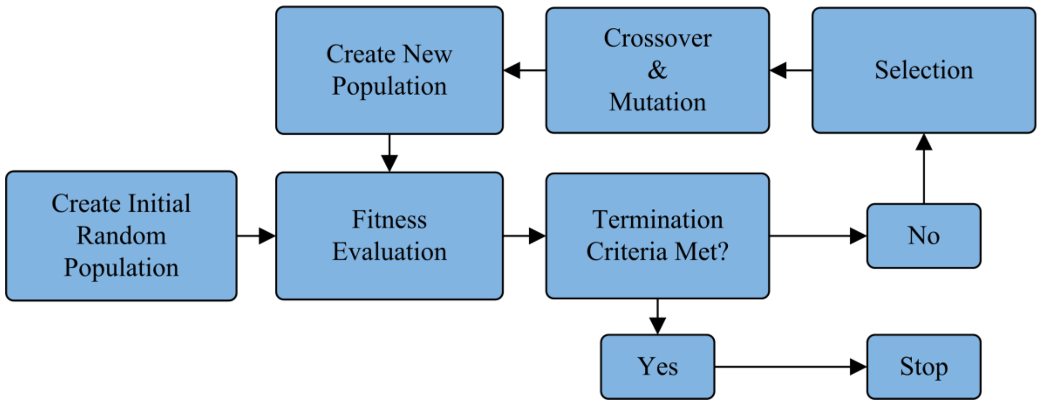

Figure 3-4: Simplified genetic algorithm optimization process. This setup reuses the best population member in the next new population (elitism), as well as reporting it to the user at each generation.

The genetic algorithm begins by creating a random set of N_{pop} chromosomes, where each population member comprises a set of input parameters encoded in a binary string. All members are evaluated and critiqued for performance based on a user-defined fitness function. In the case here, population members are evaluated by using the PFEBI program and extracting performance measures such as S-parameters and gain. Ultimately, the goal of the algorithm is to maximize the value of the fitness function by finding the optimum set of input parameters (i.e. antenna geometry). If the fitness goal is met, or other termination criteria occur, then the algorithm exits. Examples of termination criteria include insufficient computational time, the maximum number of generations has been met, or no fitness improvements have been met in an extended number of algorithm iterations, signifying convergence.

If none of the criteria for termination are met, the algorithm continues on with a process called *selection*. There are several different ways to perform the selection process. One common way is called *tournament* selection, which is implemented in the GA used here. In tournament selection, groups of population members are randomly formed and the best member of each group is retained to be a parent of the next stage. This process is repeated until enough parents are gathered for *crossover* and *mutation*.

Crossover, sometimes called mating, is the following process in the optimization cycle. It is intended to create children that have properties of both of their parents, similar to the natural process of reproduction. In crossover, a set of chromosomes from a pair (or more) of parents are blended together to form children, which can be done in numerous ways. One common way to do this is to randomly determine a point in the binary chromosome at which the parents switch. Shown in Figure 3-5, the single point crossover offers a child with properties with similarities to each parent, dependent on the crossover point.

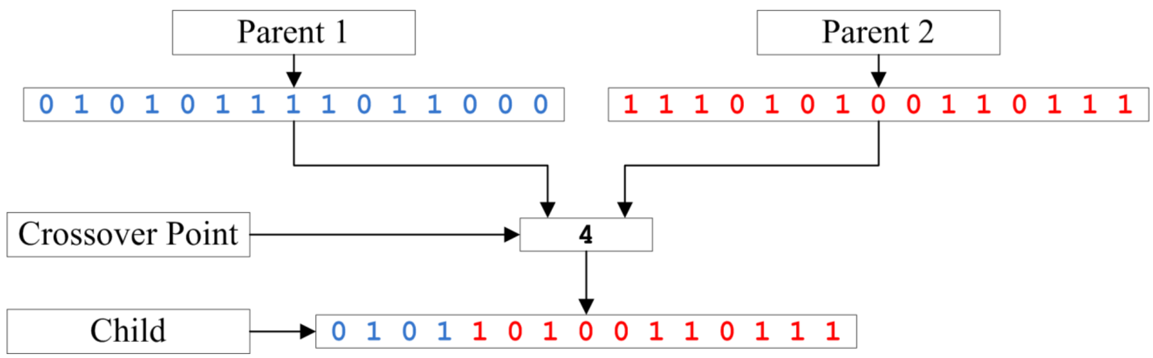

Figure 3-5: Illustration of single-point binary crossover with sample 15-bit chromosome parents and a crossover point of four.

Another common crossover type is called *uniform crossover*, where the child also has properties of both parents, but it is determined by a *crossover mask*. An example of this is shown in Figure 3-6. The crossover mask determines, for each child's chromosome bit, which parent the bit comes from. In this manner, each child can have more than two parents, although two parents are most commonly used. Uniform crossover is typically used in the antenna optimizations here and was used in the examples presented in the next chapter.

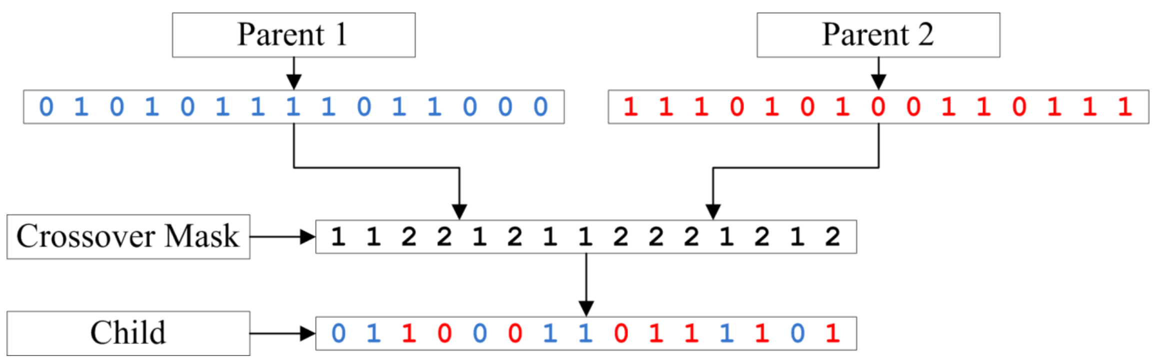

Figure 3-6: Illustration of uniform crossover with sample 15-bit chromosome parents and a randomly chosen crossover mask.

After the crossover process, the next step is *mutation*. The purpose of mutation is to increase the genetic diversity of the population. This is done by random flipping of bits in the chromosome, with mutation rates according to a user-specified probability of mutation. A balance must be chosen in mutation to avoid premature convergence (with too little mutation) and conversely, genetic drift (with too much mutation) [32].

After crossover and mutation, the population is ready for the next round of fitness evaluations. One complete cycle of these processes is called a generation, and often many generations are needed to effectively solve a problem. If the problem is badly formed or unsolvable, then it must be reformulated until it is. In the case here, this would be done by changing to a different type of antenna geometry or by reducing the demands of the fitness function.

3. 2. 5. Antenna Geometry Design Methods

The intermediate mapping of genetic algorithm parameters to antenna geometry is a critical step in effectively creating an antenna. There are many possible ways in which the metal and materials can be organized in the antennas. Initially, the metal was restricted to rectangles to form patches and basic shapes [33]. Then, pixelizations were introduced where complex metallic shapes could be optimized. Later, the pixels were grouped together to reduce the variability of designs, which especially helped to find a solution faster with the typical 60 by 60 X-Y grid sizes [34].

Initial metallic patch arrangement was done using *bit-pixelization* as shown in Figure 3-7. That is, a bit in the chromosome signified if metal would be present on the surface of a finite element. This method works well in conjunction with the genetic algorithm where binary is the natural representation. However, when a fine FE mesh becomes necessary for accuracy reasons, the number of bits required to encode a surface can become quite staggering. Additionally, the electromagnetic impact of each metal pixel becomes less significant as they become smaller. For these reasons, metallic pixels were grouped together such that a single bit would control the on-off state of the whole group, with 4 to 16 being the typical number of pixels controlled per bit. This reduces the total GA chromosome length significantly, making the optimization problem much easier to solve.

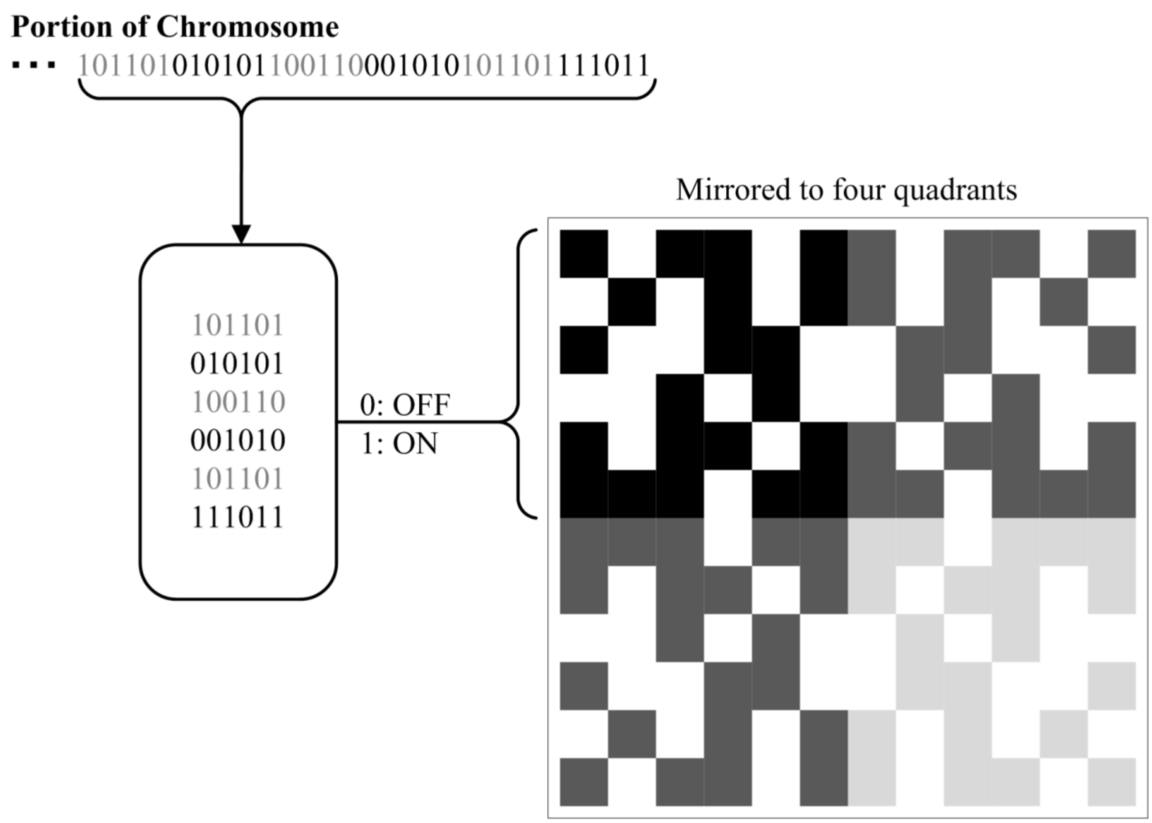

Figure 3-7: Illustration of bit-pixelization with a 6x6 grid, requiring 36 total bits for full representation of the metal surface.

In additional to standard bit-pixelization, more complex features have been integrated into the geometry mapping code. One being the inclusion of polygon-shaped metal areas and apertures, where an entire screen (horizontal surface) is filled with metal and whatever pixels are inside the shape are removed of that metal. This allows for non-rectangular shaped apertures such as bowties and dumbbells, which improves coupling can enhance antenna bandwidth [35]-

[36]. The opposite is also allowed for a bowtie shaped metal structure in place of a rectangular patch, for example.

Another structural design concept implemented into optimizations was a non-bit pixelized way of variable metal surfaces, for purposes here called a *surface function*. Similar to [37], where special polynomials controlled antenna excitation, the surface functions are used to easily control the location of metal. These methods both attempt to reduce the optimization problem dimension by having a small set of parameters that control many larger effects.

With a surface function, a two-dimensional surface is created using a small set of input variables with a truncated Fourier series. A threshold value is set, and whatever pixels are above the threshold become metal, while the ones below the threshold value remained non-metal. An example of this is shown in Figure 3-8. If the surface is mirrored doubly about the center of the intended antenna surface (which is typically the case), the metallic surface of the antenna would be as shown in Figure 3-9. The two truncated Fourier series used to create the surface function are shown in (3-1) and (3-2), where the amplitude and phase of the harmonics are controlled with the set of parameters: a, b, φ_x, and φ_y. Each of these parameters are typically encoded in 2 to 3 bits of the chromosome via standard binary quantization.

The surface function is normalized to $0 \leq S(n,m) \leq 1$ so that the threshold (which ranges from 0 to 1) can span the full range of the surface, creating anything from no metal to fully filled metal. The function is mapped to P_X by P_Y pixels, which can cover up to a full planar surface if desired, or it can be inset a certain number of pixels to prevent metallic patches from touching neighboring unit cells. Each function f and g can be created by using multiple harmonics of the fundamental, where the fundamental frequency period is twice the length of the metallic area. The x-dimension has H_X harmonics and the y-dimension has H_Y harmonics. The number of parameters to be controlled by the GA increases as the number of harmonics increase, however, therefore only a few harmonics are typically chosen for each surface.

$$f(n) = \sum_{p=1}^{H_X} a_p \cos\left(\pi\left(\frac{n-1}{P_X} + \phi_{x,p}\right)\right), \quad 1 \le n \le P_X \tag{3-1}$$

$$g(m) = \sum_{q=1}^{H_Y} b_q \cos\left(\pi\left(\frac{m-1}{P_Y} + \phi_{y,q}\right)\right), \quad 1 \le m \le P_Y \tag{3-2}$$

$$S(n,m) = f(n) \cdot g(m) \tag{3-3}$$

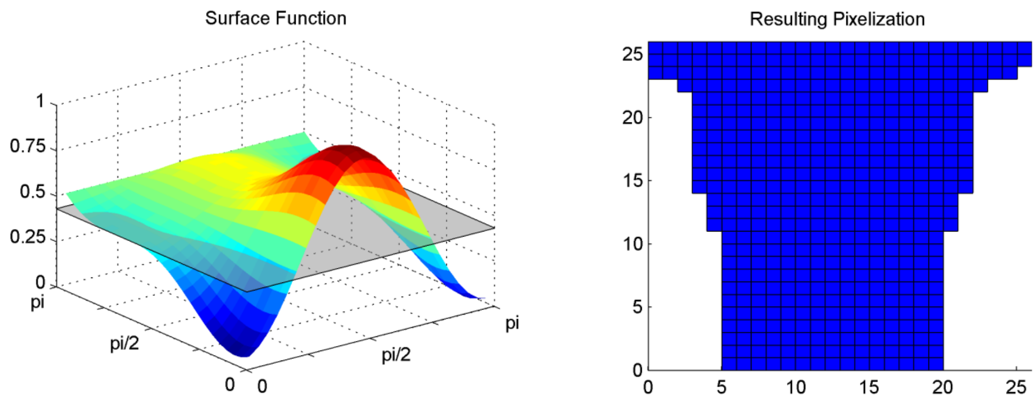

Figure 3-8: The example 2-D surface function is shown on the right, with the threshold value represented in gray. The areas where the function is greater than the threshold are mapped to metal (blue, right).

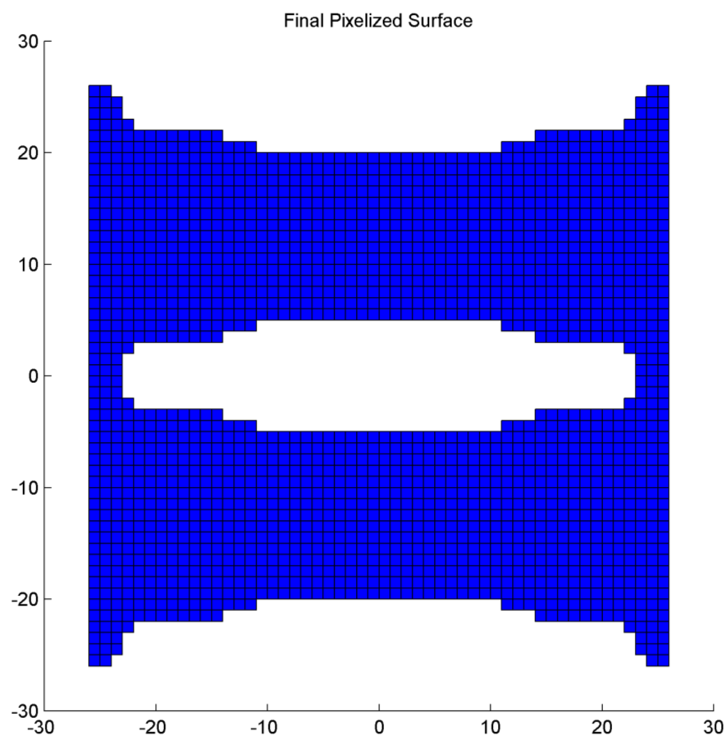

Figure 3-9: Resulting metallic surface of the surface function shown in Figure 3-8 if the metal is mirrored doubly about the origin (0,0) to a 60 by 60 X-Y grid.

In addition to placing metal horizontally on the surfaces of the materials, it can also be advantageous to create vertical pixels of metal to allow conductivity between layers or to enclose objects. This is used in some designs to create a cavity for the entire antenna or just the microstrip layer to reside. The cavity structure aids in reducing surface waves and mutual coupling between neighboring antennas [38]-[39]. It can be inexpensively realized by a closely-spaced series of vias.

Chapter 4

Optimized Design Examples

Several designs were optimized using the techniques and considerations presented in the previous chapter. Antennas were optimized on a computer cluster with software that allows parallel fitness evaluations, significantly reducing the time required for optimizations. Because of the parallel nature of the simulations, it is advantageous to use population sizes that are a multiple of the number of processors, minimizing wasted CPU time. Two examples will be shown here, one designed for use in the C-Band (Example A), and the other designed for use in the X-Band (Example B).

4. 1. Example Design A

The first antenna shown here is designed to be operated from 4.5 GHz to 5.5 GHz with a 35° conical scan. The genetic algorithm and antenna design settings for example A are shown in Table 4-1 and Table 4-2. When these settings are parameterized for placement into the genetic algorithm, they require the set of 24 variables, shown in Table 4-3. The optimized values are also shown, which required 137 generations to find with the fitness function in (4-1) and fitness settings shown in Table 4-4.

Setting	**Value**
Population Size	76 (19 processors used)
Mutation Probability	0.02
Crossover Probability	0.5
Elitism	Yes
Crossover Method	Uniform
Number of Children per Pair of Parents	1

Table 4-1: Genetic algorithm optimization settings for antenna design example A.

Criteria	Value	Comments
Unit Cell Dimension	2.4 cm x 2.4 cm	
Unit Cell Discretization	60 by 60 pixels	in the X-Y domain
Number of Physical Material Layers	4	
Range of Material Dielectric Permittivity	1.8 to 3.5	Optimized values
Material Thickness Ranges		
Top Layer	0.3 mm to 1 mm	Optimized value
Layer 2	0.3 mm to 1 mm	Optimized value
Layer 3	0.3 mm to 1 mm	Optimized value
Bottom Layer	0.5 mm	Fixed value
Metallic Structures		
Top Surface	Bit-Pixelized	6 by 6 groups of 16 pixels/quadrant
Surface 2	Bit-Pixelized	6 by 6 groups of 16 pixels/quadrant
Surface 3	Rectangular aperture	Optimized dimensions
Surface 4	Stripline feed	Optimized dimensions
Bottom Surface	Solid ground plane	
Metallic Cavity	Spans bottom 2 layers	

Table 4-2: Antenna design criteria and geometry specifications for antenna design example A.

#	Description	Min.	Max.	Possible Values (Bits Required)		Optimized Value (Binary Repres.)	
1	Material Layer 1 Thickness	0.03 cm	0.10 cm	8	(3)	0.10 cm	
2	Material Layer 1 Permittivity	1.8	3.5	8	(3)	1.8	
3	Material Layer 4 Permittivity	1.8	3.5	8	(3)	3.01	
4	Material Layer 3 Thickness	0.03 cm	0.10 cm	8	(3)	0.04 cm	
5	Material Layer 3 Permittivity	1.8	3.5	8	(3)	2.53	
6	Surface 3 Aperture Y-Origin	20	40	21	(6)	20	
7	Surface 3 Aperture X-Size	18	50	33	(6)	34	
8	Surface 3 Aperture Y-Size	4	15	12	(4)	4	
9	Surface 4 Feed X-Size	3	15	13	(4)	4	
10	Surface 4 Feed Y-Size	10	50	41	(6)	36	
11	Material Layer 2 Thickness	0.03 cm	0.10 cm	8	(3)	0.10 cm	
12	Material Layer 2 Permittivity	1.8	3.5	8	(3)	1.8	
13	Surface 1 Bit-Pixelization, Row 1	0	63	64	(6)	18	(010010)
14	Surface 1 Bit-Pixelization, Row 2	0	63	64	(6)	53	(110101)
15	Surface 1 Bit-Pixelization, Row 3	0	63	64	(6)	63	(111111)
16	Surface 1 Bit-Pixelization, Row 4	0	63	64	(6)	61	(111101)
17	Surface 1 Bit-Pixelization, Row 5	0	63	64	(6)	47	(101111)
18	Surface 1 Bit-Pixelization, Row 6	0	63	64	(6)	47	(101111)
19	Surface 2 Bit-Pixelization, Row 1	0	63	64	(6)	39	(100111)
20	Surface 2 Bit-Pixelization, Row 2	0	63	64	(6)	40	(101000)
21	Surface 2 Bit-Pixelization, Row 3	0	63	64	(6)	39	(100111)
22	Surface 2 Bit-Pixelization, Row 4	0	63	64	(6)	20	(010100)
23	Surface 2 Bit-Pixelization, Row 5	0	63	64	(6)	49	(110001)
24	Surface 2 Bit-Pixelization, Row 6	0	63	64	(6)	40	(101000)

Table 4-3: Optimizable parameters for example antenna design A. Parameter ranges are given, along with possible values and the number of chromosome bits required for representation. Binary representations of the optimized metallic bit-pixelization parameters are shown since they closely relate to the antenna geometry. For physical dimension where a unit is not given, the parameter is in pixels. Chromosome has a total length of 119 bits.

$$fitness_A = \frac{1}{\sigma_S + \sigma_G + \sigma_X} \tag{4-1}$$

$$\sigma_S = \sum_{n=1}^{N_f}\sum_{m=1}^{N_s}\begin{bmatrix} 0 & if\ \ S11_{m,n}^{simulated} \le S11_{m,n}^{goal} \\ \kappa_S\left(S11_{m,n}^{simulated} - S11_{m,n}^{goal}\right)^{\gamma_S} & otherwise \end{bmatrix} \tag{4-2}$$

$$\sigma_G = \sum_{n=1}^{N_f}\sum_{m=1}^{N_s}\begin{bmatrix} 0 & if\ \ Gain_{m,n}^{simulated} \ge Gain_{m,n}^{goal} \\ \kappa_G\left(Gain_{m,n}^{goal} - Gain_{m,n}^{simulated}\right)^{\gamma_G} & otherwise \end{bmatrix} \tag{4-3}$$

$$\sigma_X = \sum_{n=1}^{N_f}\sum_{m=1}^{N_s}\begin{bmatrix} 0 & if\ \ Xpol_{m,n}^{simulated} \le Xpol_{m,n}^{goal} \\ \kappa_X\left(Xpol_{m,n}^{simulated} - Xpol_{m,n}^{goal}\right)^{\gamma_X} & otherwise \end{bmatrix} \tag{4-4}$$

Symbol	**Fitness Parameter**	**Value**	**Comments**
$S11_{m,n}^{simulated}$	Simulated Input Return Loss	-	
$S11_{m,n}^{goal}$	Return Loss Goal	-12 dB -10 dB	At broadside When array is scanned
γ_S	Return Loss Balancing Term	1.8	
κ_S	Return Loss Weight	1.0	
$Gain_{m,n}^{goal}$	Co-polarized Broadside Gain Goal	6 dB 3 dB	At broadside When array is scanned
$Gain_{m,n}^{simulated}$	Simulated Co-polarized Broadside Goal	-	
γ_G	Co-polarized Gain Balancing Term	1.0	
κ_G	Co-polarized Gain Weight	1.0	
$Xpol_{m,n}^{simulated}$	Simulated Cross-polarized Broadside Gain	-	
$Xpol_{m,n}^{goal}$	Cross-polarized Broadside Gain Goal	-50 dB	
γ_X	Cross-polarized Gain Balancing Term	1.0	
κ_X	Co-polarized Gain Weight	1.0	

Table 4-4: Optimization fitness setting for example antenna design A.

Since the arrays are designed to operate at scan angles other than broadside, they must be simulated at each frequency (N_f) and each scan angle (N_s) for a total of $N_f \cdot N_s$ simulations per fitness evaluation. The fitness function has provisions for different return loss, co-polarized gain, and cross-polarized gain goals at different scan angles and frequencies. It is usually difficult to obtain scanned-array return losses as good as those at broadside due to increased mutual coupling, therefore the goals are typically adjusted for this. Low cross-polarized gain is specified to ensure strong linear polarization (high axial ratio). This C-Band design was optimized at the frequencies and scan angles shown in Table 4-5.

m	**Φ–Scan Direction**	**θ–Scan Direction**
1	0°	0°
2	0°	35°
3	90°	35°

n	**Frequency**
1	4.50 GHz
2	4.75 GHz
3	5.00 GHz
4	5.25 GHz
5	5.50 GHz

Table 4-5: Simulation and optimizations points for antenna example design A. A 35° conical scan was desired, therefore simulations in both the E and H planes at θ = 35° are required to give adequate performance expectations in the rest of the scan cone.

At each of the 137 generations, 15 simulations were required; each simulation can take about 1.5 to 3.0 minutes to complete, depending on the thickness and other geometry features of the structure. Because of this significant function evaluation time, it would take an intractable amount of time to find a suitable antenna design using enumerative techniques; an optimization technique is the most practical way to solve this problem. At the 137th generation, the maximum fitness value was 0.20853 with the optimized parameters as shown in Table 4-3. An additional 20 generations were ran to ensure that the GA had converged.

The final antenna performance is shown in Table 4-6 and Table 4-7. After optimization, the antenna design is simulated over the entire frequency band of interest at each scan angle. The same is done using Ansoft HFSS™ under the same frequency and scanning conditions. These frequency sweeps are shown in Figure 4-1, Figure 4-2, and Figure 4-3, showing fairly good agreement between PFEBI and HFSS™.

Frequency	**Return Loss at Φ = 0°, θ = 0°**	**Return Loss at Φ = 0°, θ = 35°**	**Return Loss at Φ = 90°, θ = 35°**
4.50 GHz	-12.9 dB	-9.5 dB	-10.5 dB
4.75 GHz	-13.8 dB	-9.2 dB	-10.4 dB
5.00 GHz	-13.2 dB	-8.7 dB	-9.3 dB
5.25 GHz	-21.0 dB	-12.8 dB	-13.2 dB
5.50 GHz	-10.6 dB	-10.3 dB	-11.5 dB

Table 4-6: Optimized return losses for example antenna design A.

Frequency	Co-pol / Cross-pol Gain at Φ = 0°, θ = 0°	Co-pol / Cross-pol Gain at Φ = 0°, θ = 35°	Co-pol / Cross-pol Gain at Φ = 90°, θ = 35°
4.50 GHz	6.7 dB / -91.4 dB	6.7 dB / -53.5 dB	6.6 dB / -92.6 dB
4.75 GHz	6.9 dB / -101 dB	6.9 dB / -55.9 dB	6.9 dB / -88.5 dB
5.00 GHz	7.2 dB / -99.1 dB	7.2 dB / -58.0 dB	7.1 dB / -88.1 dB
5.25 GHz	7.4 dB / -80.0 dB	7.4 dB / -56.6 dB	7.3 dB / -80.1 dB
5.50 GHz	7.7 dB / -67.2 dB	7.7 dB / -56.7 dB	7.6 dB / -68.9 dB

Table 4-7: Optimized gains for antenna design example A. Gains do not include input efficiency.

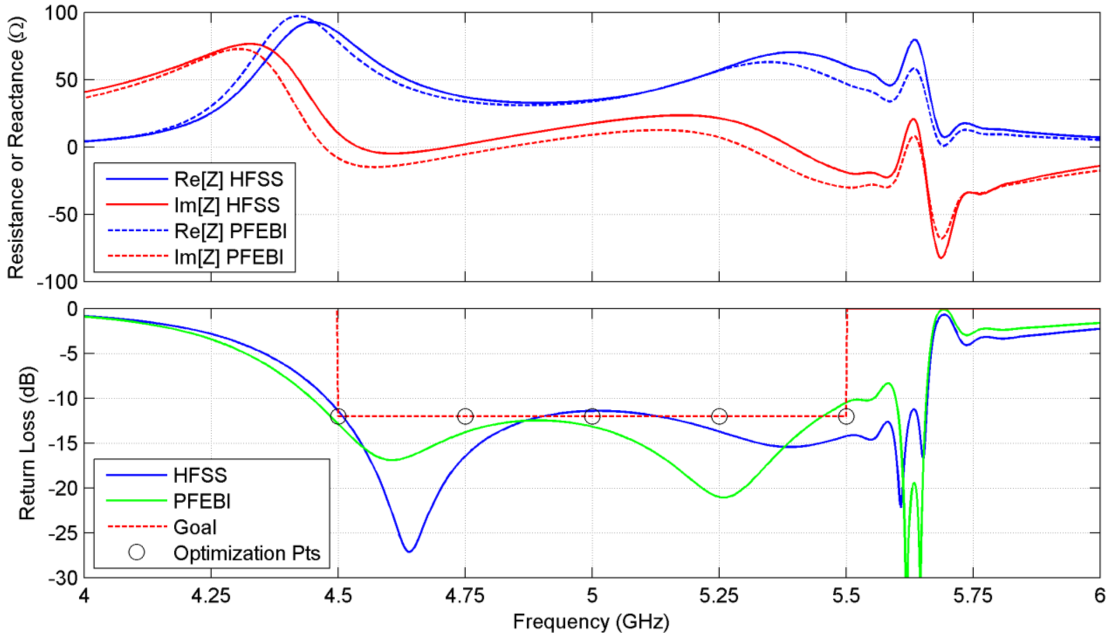

Figure 4-1: Input impedance and return loss of the optimized example antenna design A at broadside. Small differences occur between PFEBI and HFSS codes. Even so, only small dip of less than 1dB above the -12 dB goal is had over the 20% bandwidth. A sharp resonance occurs around 5.65 GHz, but it is out-of-band.

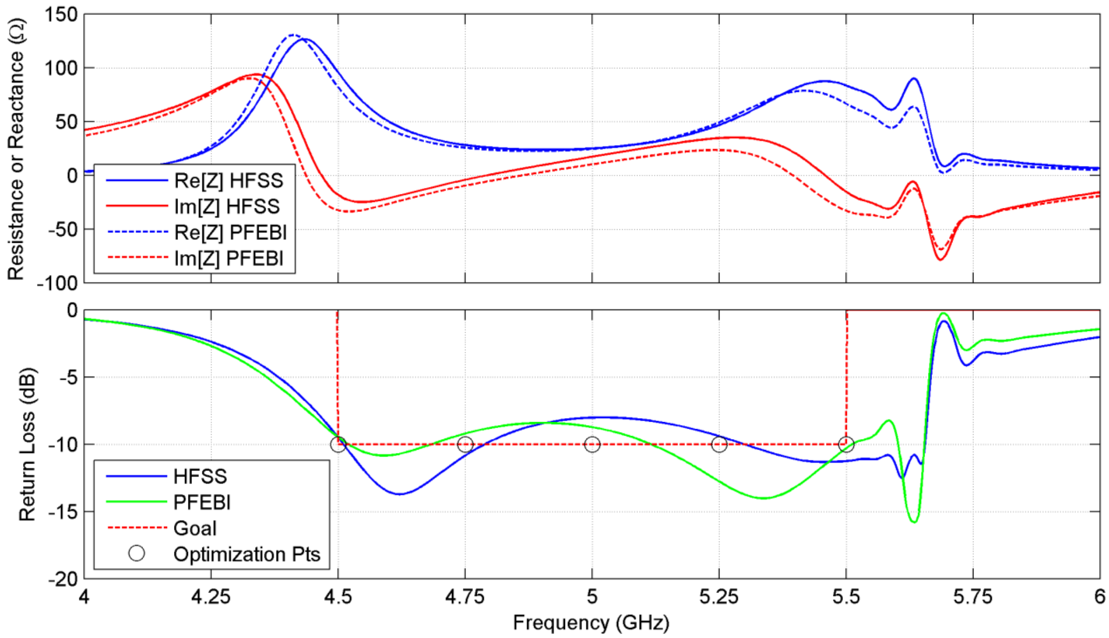

Figure 4-2: Input impedance and return loss of the optimized example antenna design A at a scan angle of $\Phi = 0°$ and $\theta = 35°$. Although the return loss is not as low as at broadside, it is still acceptable for this wide bandwidth. Better return loss can be had with narrow band and lower scan angle designs.

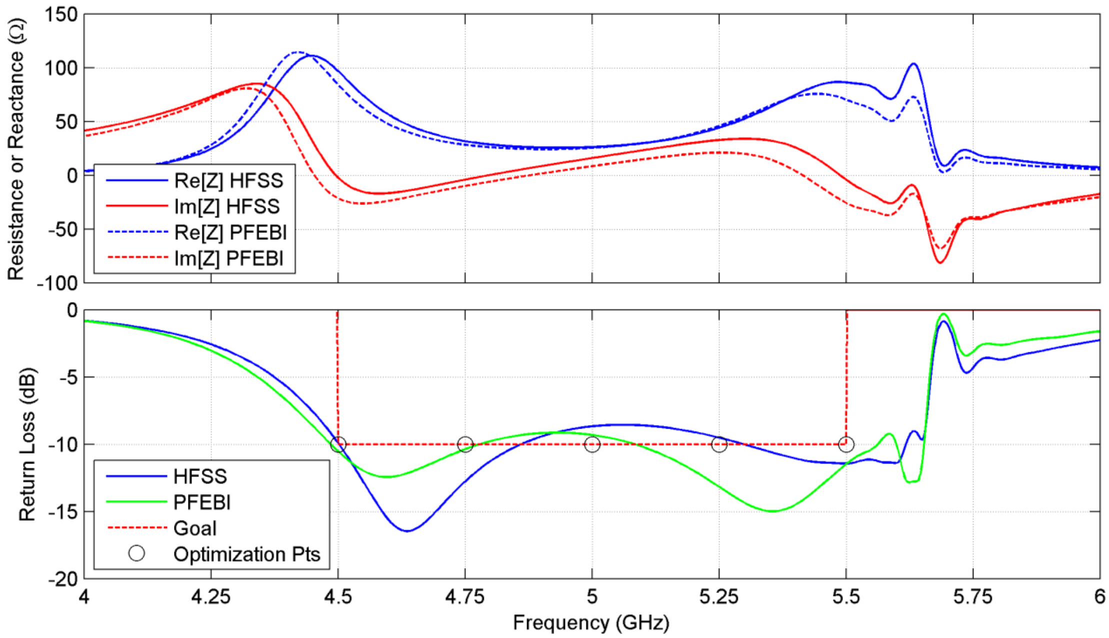

Figure 4-3: Input impedance and return loss of the optimized example antenna design A at a scan angle of $\Phi = 90°$ and $\theta = 35°$. Again, return loss is not as low as that at broadside, but this is to be expected.

The gain of the antenna does not vary as abruptly as return loss versus frequency. The fairly constant gain figures in Table 4-7 can be used as guidelines with array factors to find any full array directivity. Then, including input efficiency from return loss, array gain can be determined. This optimized antenna example provides a usable bandwidth of 20% with a 35° conical scan, all while maintaining a small thickness of 0.29 cm or $0.05\lambda_0$ (where λ_0 is free space wavelength) at the maximum operating frequency of 5.5 GHz. Layered cutaways of the optimized antenna are shown in Figure 4-4.

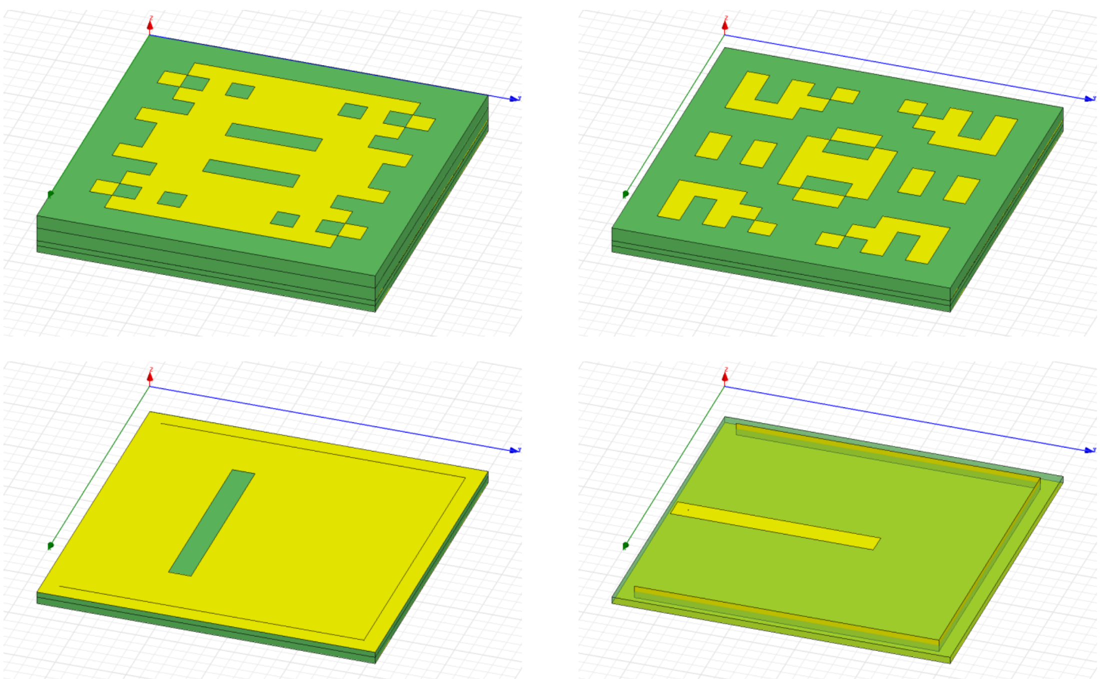

Figure 4-4: Cutaways of optimized example antenna A. Green represents substrate material and gold represents copper. Top left shows the first layer of metal pixelization, the second layer of metal pixelization is shown in top right. Rectangular aperture and cavity enclosed feed line are shown in bottom left and bottom right, respectively. Input probe is located near the edge of the unit cell between the ground plane and the feed line.

4. 2. Example Design B

In nearly the same manner as design A was optimized, another antenna for use in the X-Band was designed to be used from 9.0 GHz to 11.0 GHz, but with a much more challenging 55° scanning cone. This optimization used an alternate method of pixelization for the upper metallic layers, the surface functions as mentioned in the previous chapter. Additionally, a bowtie-shaped aperture is used instead of the standard rectangular type in attempt to provide a wider bandwidth than would normally be obtained with a standard rectangular aperture. Genetic algorithm settings are shown in Table 4-8 and antenna design specifics are shown in Table 4-9. The set of input parameters and their optimized values are shown in Table 4-14. The GA required 192 generations with 120 population members to achieve a fitness value of -1.995 with the function shown in (4-5). A modified version of the fitness function is used in attempt to give a more linear fitness relationship (as opposed to the inverse relationship with the previous fitness function). The optimized design cutaways are shown in Figure 4-8.

As with example A, full frequency sweeps at the scan angles of interest were performed and are shown in Figure 4-5, Figure 4-6, and Figure 4-7. It can be seen that even though the bandwidth of this design is the same as example A, the return loss goals are not as low. This is due to the much more difficult maximum scan angle of $\theta = 55°$, where a -6 dB return loss goal is set because of the anticipated increase in mutual coupling effects. This goal is fully met at $\Phi = 90°$ and $\theta = 55°$ but not quite at $\Phi = 0°$ and $\theta = 55°$. Even so, the antenna would be quite usable and is still relatively thin at 0.206 cm or 0.075 λ_0 at the highest operating frequency of 11 GHz.

Setting	Value
Population Size	120
Mutation Probability	0.01
Crossover Probability	0.5
Elitism	Yes
Crossover Method	Uniform
Number of Children per Pair of Parents	1

Table 4-8: Genetic algorithm optimization settings for antenna design example B.

Criteria	Value	Comments
Unit Cell Dimension	1.3 cm x 1.3 cm	
Unit Cell Discretization	60 by 60 pixels	in the X-Y domain
Number of Physical Material Layers	4	
Range of Material Dielectric Permittivity	1.8 to 3.0	Optimized values
Material Thickness Ranges		
Top Layer	0.2 mm to 0.6 mm	Optimized value
Layer 2	0.2 mm to 0.6 mm	Optimized value
Layer 3	0.2 mm to 0.6 mm	Optimized value
Bottom Layer	0.2 mm to 0.6 mm	Optimized value
Metallic Structures		
Top Surface	Surface Function	2 harmonics, 8 bits/harmonic
Surface 2	Surface Function	2 harmonics, 8 bits/harmonic
Surface 3	Bowtie aperture	Optimized dimensions
Surface 4	Stripline feed	Optimized dimensions
Bottom Surface	Solid ground plane	
Metallic Cavity	Spans bottom 2 layers	

Table 4-9: Antenna design criteria and geometry specifications for antenna design example B.

$$fitness_B = -(\sigma_S + \sigma_G + \sigma_X) \tag{4-5}$$

$$\sigma_S = \sum_{n=1}^{N_f} \sum_{m=1}^{N_s} \begin{bmatrix} 0 & if \;\; S11_{m,n}^{simulated} \le S11_{m,n}^{goal} \\ \kappa_S \left(S11_{m,n}^{simulated} - S11_{m,n}^{goal} \right)^{\gamma_S} & otherwise \end{bmatrix} \tag{4-6}$$

$$\sigma_G = \sum_{n=1}^{N_f} \sum_{m=1}^{N_s} \begin{bmatrix} 0 & if \;\; Gain_{m,n}^{simulated} \ge Gain_{m,n}^{goal} \\ \kappa_G \left(Gain_{m,n}^{goal} - Gain_{m,n}^{simulated} \right)^{\gamma_G} & otherwise \end{bmatrix} \tag{4-7}$$

$$\sigma_X = \sum_{n=1}^{N_f} \sum_{m=1}^{N_s} \begin{bmatrix} 0 & if \;\; Xpol_{m,n}^{simulated} \le Xpol_{m,n}^{goal} \\ \kappa_X \left(Xpol_{m,n}^{simulated} - Xpol_{m,n}^{goal} \right)^{\gamma_X} & otherwise \end{bmatrix} \tag{4-8}$$

Symbol	Fitness Parameter	Value	Comments
$S11_{m,n}^{simulated}$	Simulated Input Return Loss	-	
$S11_{m,n}^{goal}$	Return Loss Goal	-10 dB -6 dB	At broadside When array is scanned
γ_S	Return Loss Balancing Term	1.8	
κ_S	Return Loss Weight	1.0	
$Gain_{m,n}^{goal}$	Co-polarized Broadside Gain Goal	5 dB 3 dB	At broadside When array is scanned
$Gain_{m,n}^{simulated}$	Simulated Co-polarized Broadside Goal	-	
γ_G	Co-polarized Gain Balancing Term	1.0	
κ_G	Co-polarized Gain Weight	1.0	
$Xpol_{m,n}^{simulated}$	Simulated Cross-polarized Broadside Gain	-	
$Xpol_{m,n}^{goal}$	Cross-polarized Broadside Gain Goal	-40 dB	
γ_X	Cross-polarized Gain Balancing Term	1.0	
κ_X	Co-polarized Gain Weight	1.0	

Table 4-10: Optimization fitness setting for example antenna design B.

m	Φ–Scan Direction	θ–Scan Direction
1	0°	0°
2	0°	55°
3	90°	55°

n	Frequency
1	9.0 GHz
2	9.5 GHz
3	10.0 GHz
4	10.5 GHz
5	11.0 GHz

Table 4-11: Simulation and optimizations points for antenna example design B. A 55° conical scan was desired, therefore simulations in both the E and H planes at θ = 55° are required to give adequate performance expectations in the rest of the scan cone.

Frequency	Return Loss at Φ = 0°, θ = 0°	Return Loss at Φ = 0°, θ = 55°	Return Loss at Φ = 90°, θ = 55°
9.0 GHz	-11.0 dB	-4.94 dB	-12.5 dB
9.5 GHz	-14.7 dB	-6.17 dB	-16.6 dB
10.0 GHz	-10.2 dB	-5.13 dB	-9.77 dB
10.5 GHz	-10.8 dB	-6.82 dB	-8.45 dB
110. GHz	-9.87 dB	-9.41 dB	-5.74 dB

Table 4-12: Optimized return losses for example antenna design B.

Frequency	Co-pol / Cross-pol Gain at $\Phi = 0°, \theta = 0°$	Co-pol / Cross-pol Gain at $\Phi = 0°, \theta = 55°$	Co-pol / Cross-pol Gain at $\Phi = 90°, \theta = 55°$
9.0 GHz	5.9 dB / -62.4 dB	5.8 dB / -48.0 dB	5.8 dB / -62.3 dB
9.5 GHz	6.1 dB / -62.9 dB	5.9 dB / -45.4 dB	6.0 dB / -50.2 dB
10.0 GHz	6.3 dB / -62.5 dB	6.1 dB / -41.1 dB	6.3 dB / -51.3 dB
10.5 GHz	6.7 dB / -55.1 dB	6.3 dB / -40.4 dB	6.6 dB / -58.8 dB
110. GHz	7.1 dB / -59.7 dB	3.5 dB / -41.8 dB	7.0 dB / -59.7 dB

Table 4-13: Optimized gains for antenna design example B. Gains do not include input efficiency.

#	Description	Min.	Max.	Possible Values (Bits Required)		Optimized Value
1	Material Layer 1 Thickness	0.02 cm	0.06 cm	8	(3)	0.06 cm
2	Material Layer 1 Permittivity	1.8	3.0	4	(2)	3.0
3	Material Layer 2 Thickness	0.02 cm	0.06 cm	8	(3)	0.06 cm
4	Material Layer 2 Permittivity	1.8	3.0	4	(2)	2.6
5	Material Layer 3 Thickness	0.02 cm	0.06 cm	8	(3)	0.06 cm
6	Material Layer 3 Permittivity	1.8	3.0	4	(2)	2.2
7	Material Layer 4 Thickness	0.02 cm	0.06 cm	8	(3)	0.0257 cm
8	Material Layer 4 Permittivity	1.8	3.0	4	(2)	1.8
9	Surface 4 Feed X-Size	4	12	9	(4)	7
10	Surface 4 Feed Y-Size	30	50	21	(5)	42
11	Surface 3 Bowtie Half-Width	15	24	10	(4)	21
12	Surface 3 Bowtie Main Height	2	8	7	(3)	4
13	Surface 3 Bowtie Edge Height	1	10	10	(4)	3
14	Surface 3 Bowtie Y-Offset	-10	10	21	(5)	-5
15	Surface 1 Pix. Harm. 1 X-Mag.	0	1	4	(2)	1.0
16	Surface 1 Pix. Harm. 1 X-Phase	0	1	4	(2)	0.33
17	Surface 1 Pix. Harm. 1 Y-Mag.	0	1	4	(2)	1.0
18	Surface 1 Pix. Harm. 1 Y-Phase	0	1	4	(2)	1.0
19	Surface 1 Pix. Harm. 2 X-Mag.	0	1	4	(2)	0.0
20	Surface 1 Pix. Harm. 2 X-Phase	0	1	4	(2)	0.67
21	Surface 1 Pix. Harm. 2 Y-Mag.	0	1	4	(2)	0.0
22	Surface 1 Pix. Harm. 2 Y-Phase	0	1	4	(2)	0.33
23	Surface 1 Pix. Threshold	0	1	64	(6)	0.67
24	Surface 2 Pix. Harm. 1 X-Mag.	0	1	4	(2)	0.67
25	Surface 2 Pix. Harm. 1 X-Phase	0	1	4	(2)	0.67
26	Surface 2 Pix. Harm. 1 Y-Mag.	0	1	4	(2)	0.0
27	Surface 2 Pix. Harm. 1 Y-Phase	0	1	4	(2)	0.67
28	Surface 2 Pix. Harm. 2 X-Mag.	0	1	4	(2)	0.67
29	Surface 2 Pix. Harm. 2 X-Phase	0	1	4	(2)	1.0
30	Surface 2 Pix. Harm. 2 Y-Mag.	0	1	4	(2)	0.33
31	Surface 2 Pix. Harm. 2 Y-Phase	0	1	4	(2)	0.67
32	Surface 2 Pix. Threshold	0	1	64	(6)	0.89

Table 4-14: Optimizable parameters for example antenna design B. Parameter ranges are given, along with possible values and the number of chromosome bits required for representation. Chromosome is 89 bits long.

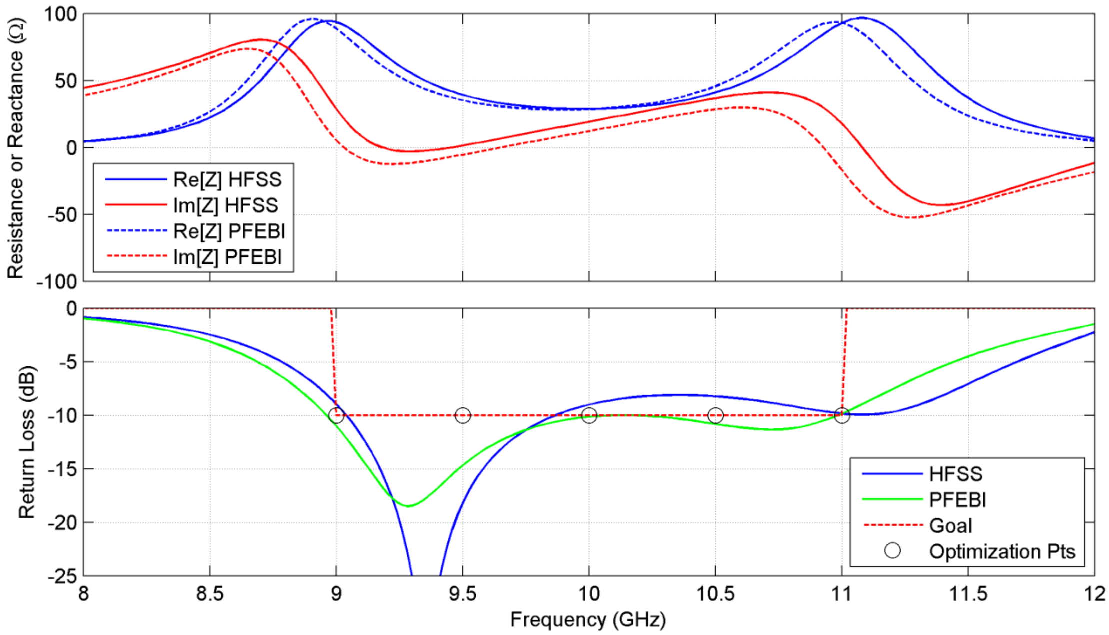

Figure 4-5: Input impedance and return loss of the optimized example antenna design B at broadside. Small differences occur between PFEBI and HFSS codes. Even so, only small dip of less than 1dB above the -12 dB goal is had over the 20% bandwidth. A sharp resonance occurs around 5.65 GHz, but it is out-of-band.

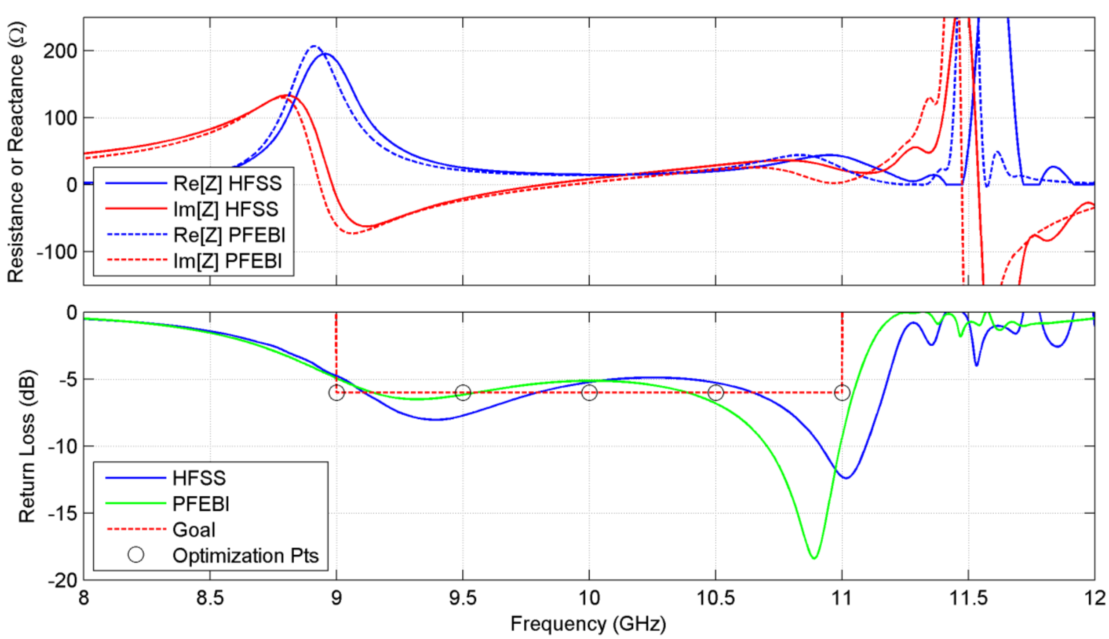

Figure 4-6: Input impedance and return loss of the optimized example antenna design B at a scan angle of $\Phi = 0°$ and $\theta = 55°$. The difficulty of low return loss at high scan angles becomes apparent. A very strong resonance is exhibited at about 11.5 GHz, but it is out-of-band.

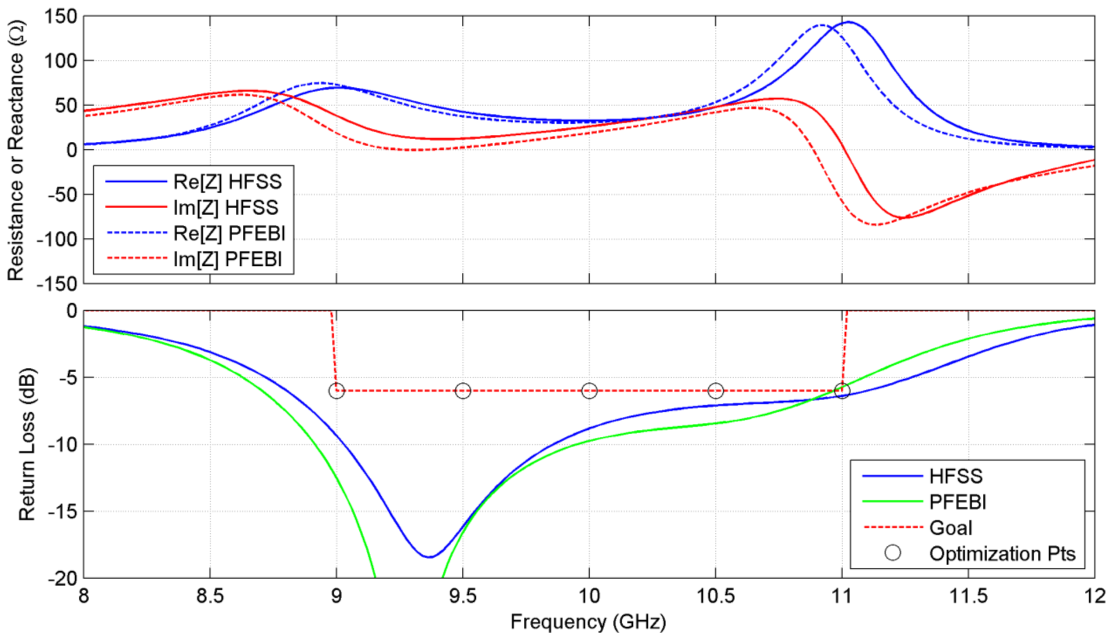

Figure 4-7: Input impedance and return loss of the optimized example antenna design B at a scan angle of $\Phi = 90°$ and $\theta = 55°$. All goals are met in both PFEBI and HFSS results.

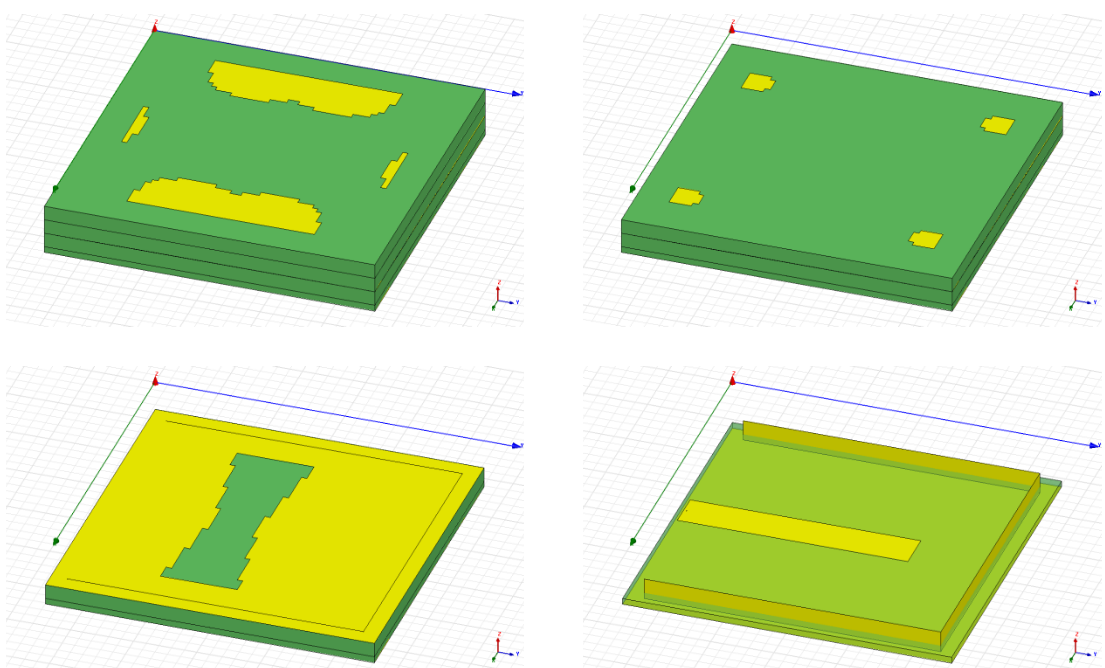

Figure 4-8: Cutaways of optimized example antenna B. Green represents substrate material and gold represents copper. Top left shows the first layer of metal pixelization, the second layer of metal pixelization is shown in top right. Bowtie-shaped aperture and cavity enclosed feed line are shown in bottom left and bottom right, respectively. Input probe is located near the edge of the unit cell between the ground plane and the feed line.

Chapter 5

Conclusions and Summary

5. 1. Polyfractal Array Verification

Both the polyfractal arrays and wideband-element periodic arrays are useful additions to the array community. Polyfractal arrays are an effective way to obtain low sidelobe levels and avoid grating lobes over extended bandwidths. It has been shown that even with real, fabricated arrays which can exhibit many non-ideal properties, they still yield the low sidelobe levels that their isotropic array factors predict. For the relatively small, 32-element polyfractal arrays, they respectively exhibit relative sidelobe levels of -16.3 dB and -14.2 dB sidelobe levels for arrays A and B at 0.5λ minimum spacing, where a periodic array would exhibit -13.2 dB. Where the polyfractal arrays become especially effective is above 1λ minimum element spacing (for an unsteered array), where a periodic array develops grating lobes (0 dB SLL). The example polyfractal arrays A and B, however, exhibit peak sidelobe levels of only about -5.4 dB each.

Even better performance can be achieved with polyfractal arrays that consist of more elements as the 1924-element example in Figure 1-5 and Figure 1-6 demonstrates, exhibiting a peak sidelobe level of -16.3 dB at 14λ minimum element spacing. The great advantage to the polyfractal design method is the customizability for creating arrays of different size and for different bandwidths, not simply being restricted to a specific array size or operating bandwidth.

5. 2. Optimization of Antenna Elements in an Infinite Array

Despite the design advantages of polyfractal and aperiodic arrays, periodic arrays can still be attractive due to ease of manufacturing. Even when heeding the element spacing restrictions of periodic arrays illustrated in chapter one, significant fractional bandwidths with thin substrates can be obtained with proper element design. The specialized PFEBI software, coupled with an optimization tool, has been used to design these elements while accounting for all effects of having them in the array, eliminating any unexpected and unknown effects of simply placing an element in an array formation. This is especially useful when elements need to be as large as possible to exhibit good low frequency performance, but must also be spaced close together to avoid grating lobes at higher frequencies.

The two example antennas were designed using the genetic algorithm and were optimized to function in two different frequency bands, one antenna for C-Band and one for X-Band. Both were optimized for a 20% bandwidth at center frequencies of 5.0 GHz and 10 GHz, the former operating up to 35° from broadside and the latter up to 55° from broadside. They provided good gain, low cross-polarization and acceptable return losses over their intended bandwidths and scan angles. In addition, many other antennas can be created with this design procedure. As with the polyfractal design method, it is the customizability that is a great advantage here; antennas can be optimized for any reasonable bandwidth and scanning angles, performances and operating frequencies are not limited to the few examples presented here.

References

[1] J. S. Petko and D.H. Werner, "The Evolution of Optimal Linear Polyfractal Arrays Using Genetic Algorithms," *IEEE Transactions on Antennas and Propagation*, Vol.53, No.11, pp. 3604-3615, Nov. 2005.

[2] J. S. Petko and D.H. Werner, "An Autopolyploidy-Based Genetic Algorithm for Enhanced Evolution of Linear Polyfractal Arrays," *IEEE Transactions on Antennas and Propagation*, Vol.55, No.3, pp.583-593, March 2007.

[3] J. S. Petko and D.H. Werner, "The Pareto Optimization of Ultrawideband Polyfractal Arrays," *IEEE Transactions on Antennas and Propagation*, Vol.56, No.1, pp.97-107, Jan. 2008.

[4] C. A. Balanis, *Antenna Theory: Analysis and Design*, 3rd ed. Hoboken, NJ: John Wiley & Sons, 2005.

[5] M. I. Skolnik, *Introduction to Radar Systems, 3rd ed.* New York, NY: McGraw-Hill, 2001.

[6] J. H. Doles and F. D. Benedict, "Broad-Band Array Design Using the Asymptotic Theory of Unequally Spaced Arrays," *IEEE Transactions on Antennas and Propagation*, Vol. 36, No. 1, Jan. 1988.

[7] Y. Kim and D.L. Jaggard, "The Fractal Random Array," *Proceedings of the IEEE*, Vol.74, No.9, pp. 1278-1280, Sept. 1986.

[8] R. L. Haupt and D. H. Werner, *Genetic Algorithms in Electromagnetics*, New Jersey: Wiley/IEEE Press, 2007.

[9] D. H. Werner, R. L. Haupt, and P. L. Werner, "Fractal Antenna Engineering: The Theory and Design of Fractal Antenna Arrays," *IEEE Antennas and Propagation Magazine*, Vol. 41, No. 5, pp. 37-58, Oct. 1999.

[10] D. M. Pozar, "Microstrip Antennas," *Proceedings of the IEEE*, Vol. 80, No. 1, Jan. 1992.

[11] Ansoft LLC, *Designer 2.2*. [Download]. Pittsburgh, PA.: Ansoft Corporation, 2005.

[12] H. A. Wheeler, "Fundamental Limitations of Small Antennas," *Proceedings of the IRE*, Dec. 1947.

[13] R. C. Hansen, "Fundamental Limitations in Antennas," *Proceedings of the IEEE*, Vol. 69, No. 2, Feb. 1981.

[14] R. P. Jedlicka, M. T. Poe, and K. R. Carver, "Measure Mutual Coupling Between Microstrip Antennas," *IEEE Transactions on Antennas and Propagation*, Vol. 29, No. 1, Jan. 1981.

[15] A. H. Mohammadian, N. M. Martin, and D. W. Griffin, "A Theoretical and Experimental Study of Mutual Coupling in Microstrip Antenna Arrays," *IEEE Transactions on Antennas and Propagation*, Vol. 37, No. 10, Oct. 1989.

[16] E. Penard and J. P. Daniel, "Mutual Coupling Between Microstrip Antennas," *IEEE Electronics Letters*, Vol. 18, No. 14, July 1982.

[17] E. H. Van Lil and A. R. Van de Capelle, "Transmission Line Model for Mutual Coupling Between Microstrip Antennas," *IEEE Transactions on Antennas and Propagation*, Vol. 32, No. 8, Aug. 1984.

[18] P. B. Katehi, "A Generalized Method for the Evaluation of Mutual Coupling in Microstrip Arrays," *IEEE Transactions on Antennas and Propagation*, Vol. 35, No. 2, Feb. 1987.

[19] C. M. Krowne, "Dielectric and Width Effect on H-Plane and E-Plane Coupling between Rectangular Microstrip Antennas," *IEEE Transactions on Antennas and Propagation*, Vol. 31, No. 1, Jan. 1983.

[20] H. Steyskal and J. S. Herd, "Mutual Coupling Compensation in Small Array Antennas," *IEEE Transactions on Antennas and Propagation*, Vol. 38, No. 12, Dec. 1990.

[21] M. A. Khayat, J. T. Williams, D. R. Jackson, and S. A. Long, "Mutual Coupling Between Reduced Surface-Wave Microstrip Antennas," *IEEE Transactions on Antennas and Propagation*, Vol. 48, No. 10, Oct. 2000.

[22] F. Yang and Y. Rahmat-Samii, "Microstrip Antennas Integrated With Electromagnetic Band-Gap (EBG) Structures: A Low Mutual Coupling Design for Array Applications," *IEEE Transactions on Antennas and Propagation*, Vol. 51, No. 10, Oct. 2003.

[23] T. Huynh and K. F. Lee, "Single-Layer Single-Patch Wideband Microstrip Antenna," *IEEE Electronics Letters*, Vol. 31, No. 16, Aug. 1995.

[24] M. Rahman and M. A. Stuchly, "Wideband Microstrip Patch Antenna with Planar PBG Structure," *IEEE Antennas and Propagation International Symposium,* Vol. 2, pp. 486-489, 2001.

[25] W. J. Lui, C. H. Cheng, Y. Cheng, and H. Zhu, "Frequency Notched Ultra-Wideband Microstrip Slot Antenna With Fractal Tuning Stub," *IEEE Electronics Letters*, Vol. 41, No. 6, Mar. 2005.

[26] A. A. Eldek, A. Z. Elsherbeni, and C. E. Smith, "Wideband Microstrip-Fed Printed Bowtie Antenna for Phased-Array Systems," *Microwave and Optical Technology Letters*, Vol. 43, No. 2, pp. 123-126, Oct. 2004.

[27] S. D. Targonski, R. B. Waterhouse, and D. M. Pozar, "Design of Wide-Band Aperture-Stacked Patch Microstrip Antennas," *IEEE Transactions on Antennas and Propagation*, Vol. 46, No. 9, Sept. 1998.

[28] L. Akhoondzadeh, D. J. Kern, P. S. Hall, and D. H. Werner, "Wideband Dipoles on Electromagnetic Bandgap Ground Materials," *IEEE Transactions on Antennas and Propagation*, Vol. 55, No. 9, Sept. 2007.

[29] J. L. Volakis, A. Chatterjee, and L. C. Kempel, *Finite Element Method for Electromagnetics*, IEEE Press, 1998.

[30] B. Thors, H. Steyskal, and H. Holter, "Broad-Band Fragmented Aperture Phased Array Element Design Using Genetic Algorithms," *IEEE Transactions on Antennas and Propagation*, Vol. 53, No. 10, Oct. 2005.

[31] Ansoft LLC, *HFSS 11.1*. [Download]. Pittsburgh, PA.: Ansoft Corporation, 2008.

[32] T. Bäck, D. B. Fogel, and Z. Michalewicz, *Handbook of Evolutionary Computation*, New York: Oxford University Press, 1997.

[33] R. K. Shaw, and D. H. Werner, "Design of Optimal Broadband Microstrip Antenna Elements in the Array Environment using Genetic Algorithms," *Proceedings of the 2006 IEEE International Symposium on Antennas and Propagation Society*, pp. 3727-3730, July 2006.

[34] M. D. Gregory and D. H. Werner, "Optimization of Broadband Antenna Elements in a Periodic Planar Infinite Array," *Proceedings of the 2009 IEEE International Symposium on Antennas and Propagation*, June, 2009.

[35] V. Rathi, G. Kumar, and K. P. Ray, "Improved Coupling for Aperture Coupled Microstrip Antennas," *IEEE Transactions on Antennas and Propagation*, Vol. 44, No. 8, Aug. 1996.

[36] D. M. Pozar, and S. D. Targonski, " Improved Coupling for Aperture Coupled Microstrip Antennas," *IEEE Electronics Letters*, Vol. 27, No. 13, June 1991.

[37] D. W. Boeringer, D. H. Werner, D. W. Machuga, "A Simultaneous Parameter Adaptation Scheme for Genetic Algorithms with Application to Phased Array Synthesis," *IEEE Transactions on Antennas and Propagation*, Vol.53, No.1, pp. 356-371, Jan. 2005.

[38] F. Zavosh and J. T. Aberle, "Single and Stacked CIrcular Microstrip Patch Antennas Backed by a Circular Cavity," *IEEE Transactions on Antennas and Propagation*, Vol. 43, No. 7, July 1995.

[39] Q. Li and Z. Shen, "Microstrip-Fed Cavity-Backed Slot Antennas," *Microwave and Optical Technology Letters*, Vol. 33, No. 4, May 2002.

Appendix A

Top Layer Copper Silhouettes of Polyfractal Prototypes

Array A at 5GHz	Array A at 20 GHz	Array B at 5 GHz	Array B at 20 GHz
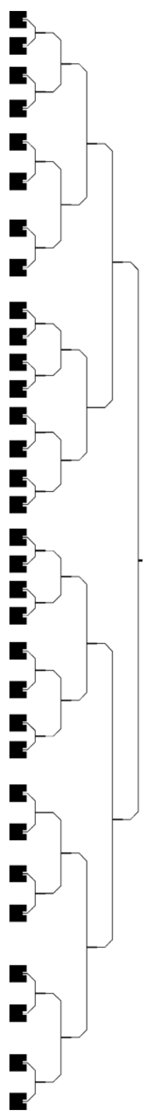	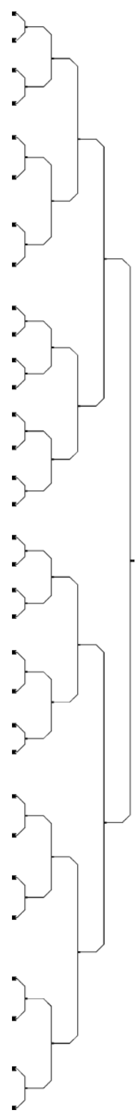	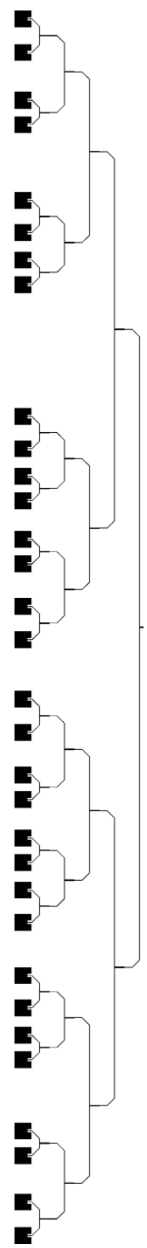	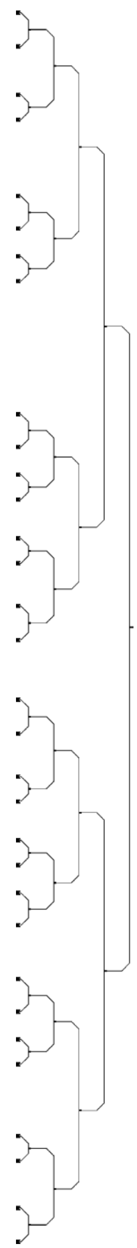

Appendix B

Fabricated Subarrays of Polyfractal Prototype Array A

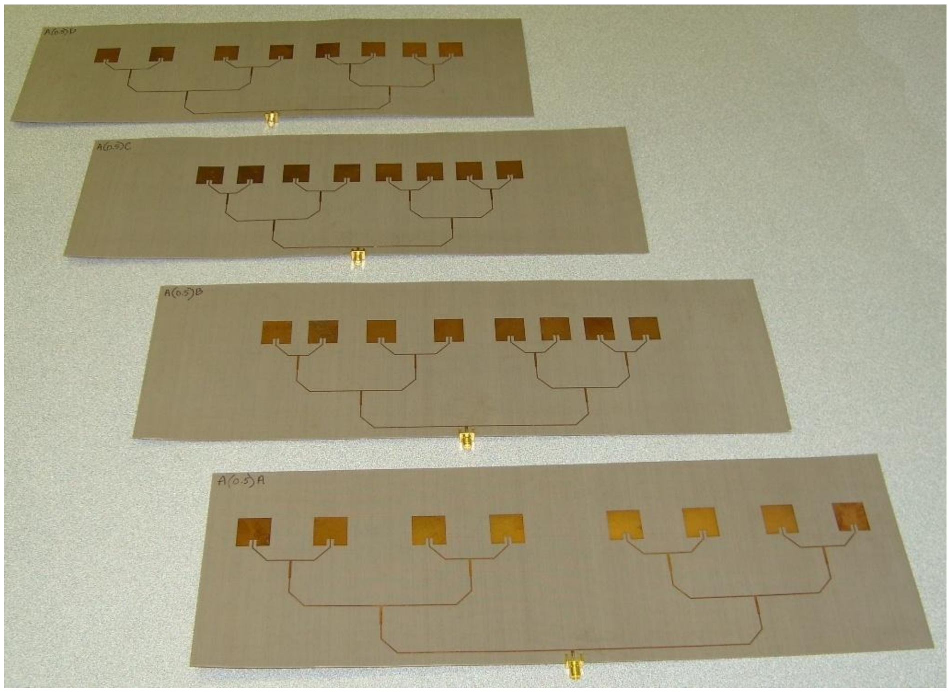

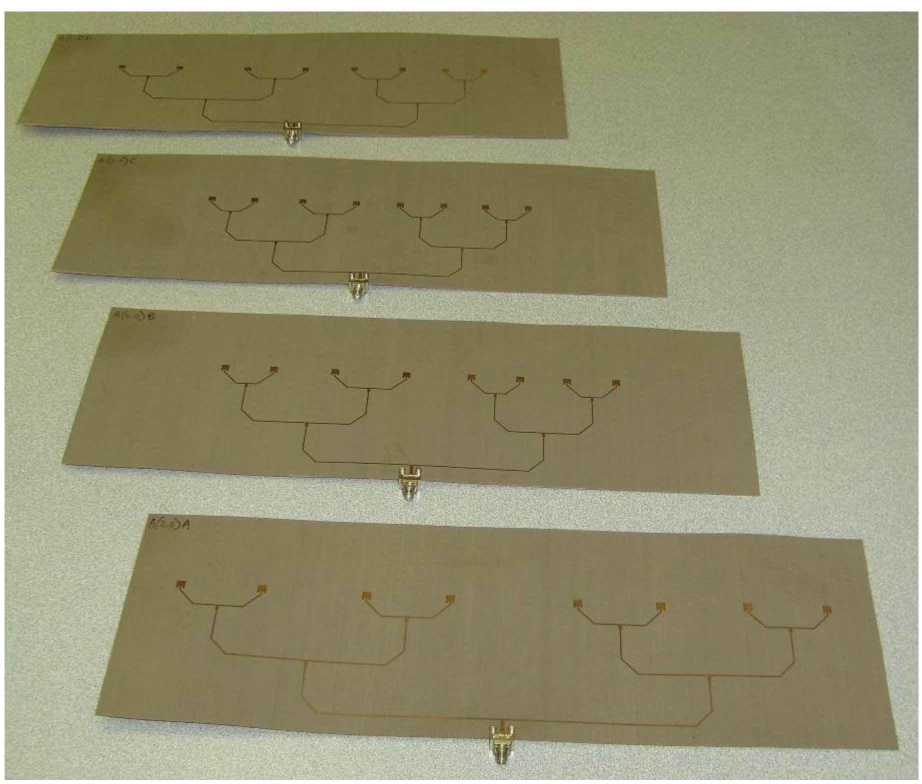

Appendix C

Fabricated Subarrays of Polyfractal Prototype Array B